Progress in Materials Science 123 (2022) 100793

Contents lists available at ScienceDirect

Progress in Materials Science

journal homepage: www.elsevier.com/locate/pmatsci

Five decades of research on the development of eutectic as engineering materials

Chandra Sekhar Tiwary [a,1], Prafull Pandey [b,1], Suman Sarkar [c], Rakesh Das [a], Sumanta Samal [d], Krishanu Biswas [e], Kamanio Chattopadhyay [b,*]

[a] Metallurgical and Materials Engineering, Indian Institute of Technology Kharagpur, West Bengal, India
[b] Materials Engineering, Indian Institute of Science, Bangalore, Karnataka, India
[c] Materials Engineering, Indian Institute of Technology Jammu, Jammu 181221, India
[d] Metallurgy Engineering and Materials Science, Indian Institute of Technology Indore, India
[e] Department of Materials Science and Engineering, Indian Institute of Technology Kanpur, Kanpur 208016, India

ARTICLE INFO

Keywords:
Eutectic alloy
Solidification
Alloy development
Microstructure
Mechanical properties

ABSTRACT

We present a brief review and perspective on the development of eutectic alloys, emphasizing the emergence of complex microstructures during eutectic solidification of ternary and higher-order multicomponent alloys. Such alloys' abundant existence promises a large domain in the alloy development space for newer materials suitable for high-temperature applications. Hence the review explores these developments in eutectic alloys based on aluminum, titanium, nickel, intermetallics, and recently developed high entropy alloys. While the importance of fundamental understanding and various functional properties of the eutectic alloys cannot be ignored, this paper focuses primarily on the microstructure and their mechanical properties. The possibilities of ultrafine eutectics and multiscale variation of length scale and morphologies are emphasized. It highlights the potential for the future emergence of these alloys as high-strength structural materials for engineering applications.

0. Personal introduction

This paper is part of a symposium in honor of Professor B. Cantor, who is well known for his contribution to developing new/innovative alloys and tuning their properties through microstructure and processing engineering. Professor Cantor worked on eutectic alloys for his Ph.D. degree, and hence it remains close to his heart. One of us (KC) worked closely with him from the early eighties on the processing, structure, and properties of non-equilibrium materials. His continuous association with our group and his active discussion on eutectic alloys' development during his several visits to the Department of Materials Engineering, Indian Institute of Science, Bangalore, is noteworthy. In this review, the team has summarized the development of eutectic alloys as an important class of structural materials.

* Corresponding author.
E-mail address: kamanio@iisc.ac.in (K. Chattopadhyay).
[1] Equal contribution.

https://doi.org/10.1016/j.pmatsci.2021.100793
Received 21 August 2020; Received in revised form 24 February 2021; Accepted 1 March 2021
Available online 9 March 2021

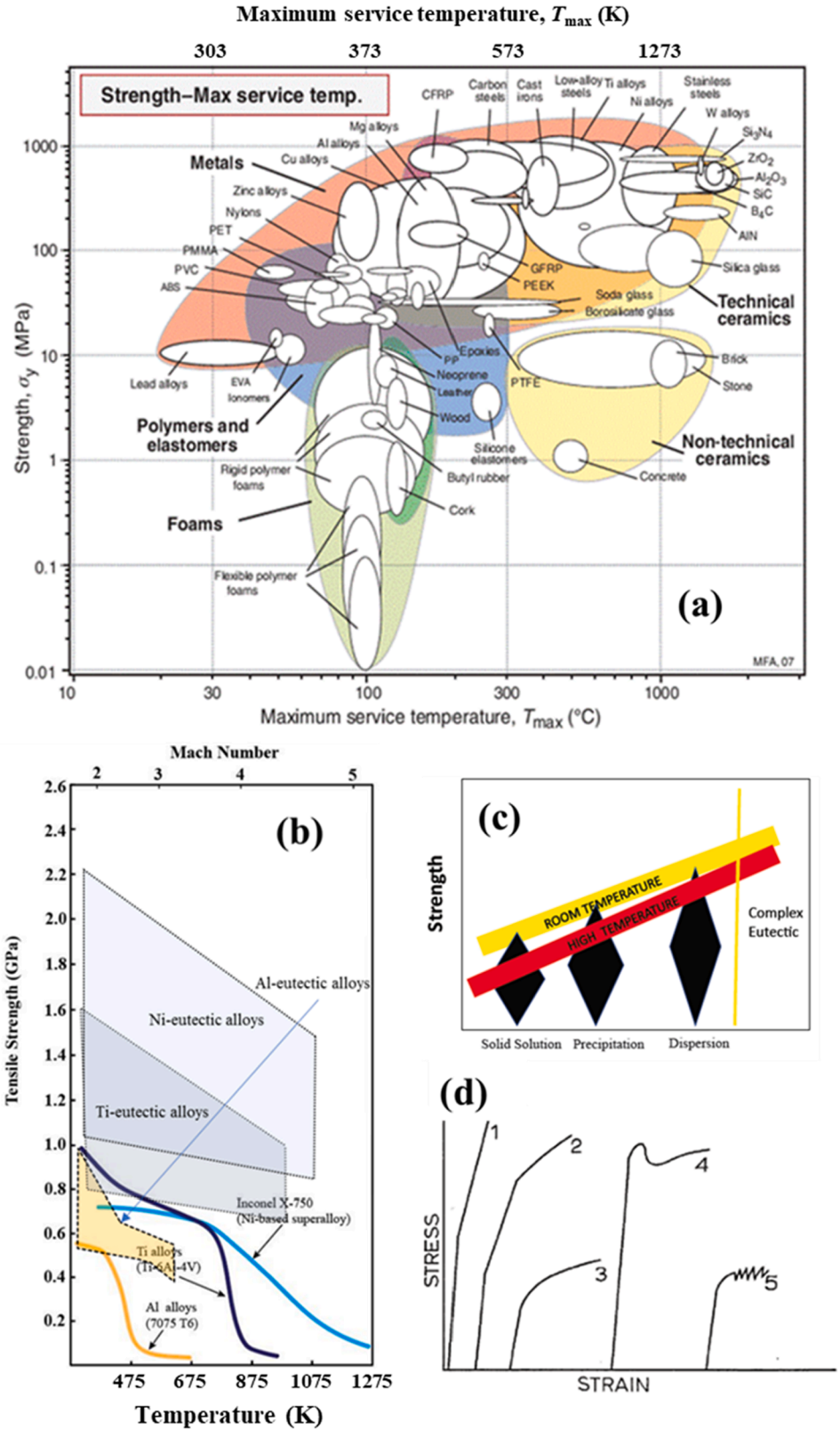

(caption on next page)

Fig. 1. (a) Strength vs. maximum service temperature Ashby map for different materials. (b) Strength vs. maximum service temperature for different structural materials and their eutectic counterpart. (c) Schematic showing strength variation at room temperature and high temperatures for different strengthening mechanisms. (d) Typical tensile stress/strain curves for eutectic alloys: (1) ductile matrix-brittle fibers or ductile matrix-brittle lamellae, (2) ductile matrix-ductile fibers, (3) ductile matrix-ductile fibers, (4) ductile matrix-brittle fibers, (5) serrated stress/strain curve for single crystal Zn-Al eutectic alloy [1].

1. Introduction

The development of structural materials is governed by the requirement/demand of its applications. The societal needs continuously push the applications' envelope (e.g., strength, application temperature, energy efficiency, etc.) that require alloys with improved properties. In the realm of structural materials, a newer class of alloys continuously emerge in the domains dominated by steels, nickel-based superalloys, aluminum and titanium alloys, and alloys like solder alloys, which have great utility in fabrication processes. The power, aerospace, and automobile industries demand materials with a low density and high strength, leading to an increasing developmental effort in the last several years. The strength (MPa) vs. density map given by Ashby is shown in Fig. 1a, depicting a range of materials available, starting from natural materials to foams. As shown, the increase in strength often compromises density. In this respect, the recent developments in polymers, elastomers, and ceramics have the edge over metals and alloys. However, for high-temperature applications, the choices are still among oxides, intermetallics, refractory alloys, and superalloys. The difficulty in processing and often poorer room temperature mechanical behavior limit the application of oxides. Among the metallic materials, the Al, Ti, and Ni-based alloys developed in the last 60 years are still potent and enables today's power generation and air travel. As the strength vs. temperature plots (Fig. 1b) show, these alloys' strength remains stable till service temperature (~473, 800 and 1100 K for Al alloys, Ti alloys, and Ni-based alloys, respectively). Most of these are designed based on strengthening mechanisms involving solid-solution, precipitation, and dispersion hardening (Fig. 1c). The basic properties (such as strength, modulus, hardness, and fracture toughness) of the second phase and its interface with the matrix govern the mechanical properties of alloys. Hence, the thrust of research in these alloy systems is directed to optimize the size, shape, and distribution of the precipitates and the nature of their interface with the matrix (coherent, semi-coherent, or incoherent). Despite all these optimizations and fine-tuning, there is a limit to which these alloys room temperature strength can be improved. With the increase in operating temperature, processes like diffusion, coarsening, and temperature-dependent modification of interfaces result in a deterioration of these alloys mechanical properties. Currently, a significant research effort is devoted to further improving these alloys. Apart from well-known strengthening mechanisms, composite strengthening (second phase reinforcement into the matrix) has also attracted considerable attention (Fig. 1b, c). Among

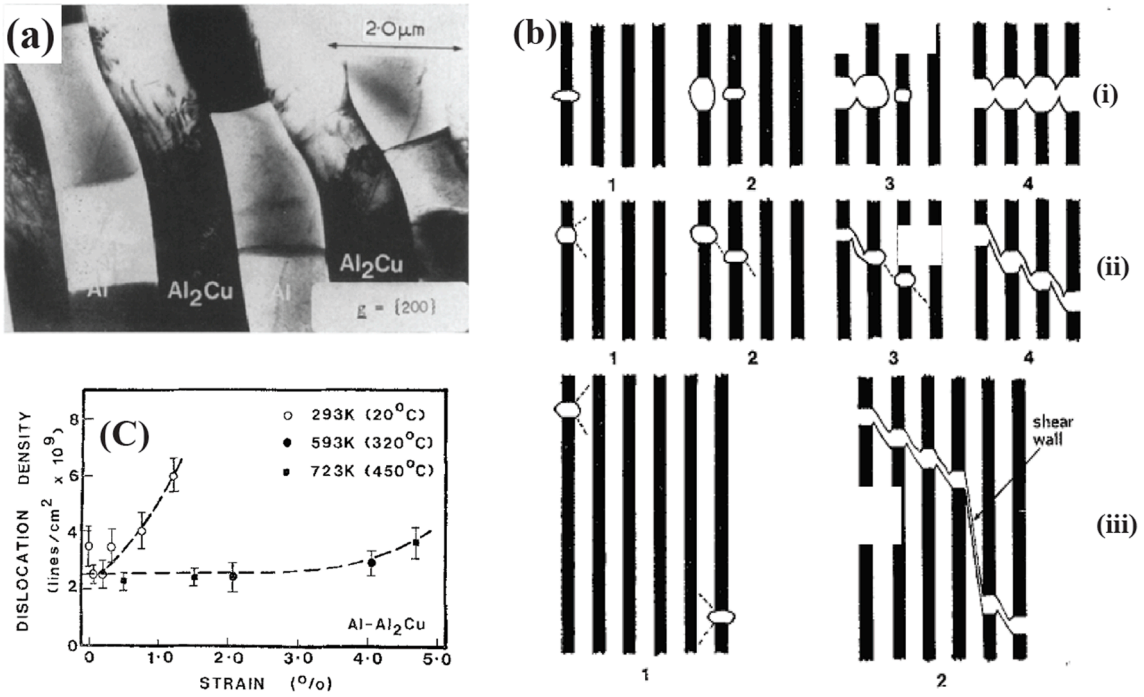

Fig. 2. (a) electron micrograph of a transverse section of Al-Al_2Cu deformed 2% in tension at 593 K. Matrix dislocations are predominantly in the form of sub-boundaries (b) Diagram of fracture modes in aligned composites. In (i) elastic stress concentration around a fiber-break causes fracture of adjacent fibers and composite failure at 90° to the tensile axis. In (ii) shear in the matrix causes fracture of adjacent fibers and composite failure at 45° to the tensile axis. In (iii), the presence of pre-cracked fibers causes shear walls in the matrix during composite failure. (c) Dislocation density as a function of strain during tensile deformation of Al-Al_3Ni eutectic single crystals [2–4].

these, eutectic alloys in which two or more phases form in a coupled manner during solidification from alloy melt demand special attention.

Several eutectic alloy systems (such as cast iron, Al-Si, Sn-Ag-Cu, etc.) are widely used in electronics, automotive, aerospace, and related industries while new applications are emerging rapidly. The strength of a eutectic alloy primarily depends on (i) the spacings among the phases (e.g., interlamellar spacing for the binary lamellar eutectic), (ii) volume fraction of the constituent phases and their mechanical properties, (iii) crystal structures of the constituent phases (iv) the nature of the interphase interfaces and (v) morphology of the phases in the eutectic microstructure. Tuning these variables allows us to substantially optimize the mechanical properties (Fig. 1d), showing that a variation of the individual lamella's nature can result in different mechanical properties. Hence, a significant part of the research is focused on developing an understanding of the structure-property correlation in eutectic alloys. These efforts till 1975 are summarized in an article in this journal by Chadwick [1]. In a series of pioneering papers published in the mid-70s, Cantor and Chadwick established the relation between mechanical deformation and microstructure in classical rod eutectic (Al-Al_3Ni) and plate eutectic (Al-Al_2Cu) [2–4] (Fig. 2a–c). These studies initiated a new area of research for the development of eutectic alloys as structural materials. In his critical assessment published in the Metal Science in 1975 [5], Chadwick highlighted the unsolved issues that need to be addressed.

Two parallel research directions are being pursued in the community working on the development of eutectic alloys. One of them is a large and vibrant community committed to understanding the fundamentals of eutectic growth through theory and experiments with pioneering contributions from Trivedi, Hunt, and Kurz & Fisher and several of their contemporaries [6–10]. These are soon followed by researchers employing phase-field simulation methodology, attempting to correlate the evolution of eutectic microstructure under different equilibrium and non-equilibrium growth conditions. Several reviews and book chapters have summarized this area of eutectic research [11–13]. An alternate direction has focussed on engineering classical and complex eutectic microstructure to obtain superior mechanical properties for applications at room and high temperatures. The current review deals with this latter approach of alloy design and will attempt to provide a perspective for future alloy developments based on eutectic strengthening.

In alloys with a microstructure consisting of a stronger eutectic matrix with or without embedded softer dendrites, the strength of the material (σ_{ye}) will be controlled by the harder phase. For a eutectic with a cooperative growth, the length scale is governed by the interlamellar (or rod) spacing (λ); a Hall-Petch like equation can be written as, $\sigma_{ye} = \sigma_{0e} + K\,\lambda^{(-1/2)}$; where σ_{ye} is the yield strength of the material, σ_{0e} is the friction stress, λ is the interlamellar spacing. It is known as the Hall-Petch equation for two-phase eutectic alloys and reflects the fact that the finer the interlamellar spacing (λ), the higher will be the strength (σ_{ye}). Therefore, it is necessary to reduce the spacing (λ) to obtain higher strength. The above suggestion has gained widespread acceptance in recent years with the emergence of nanoscale or ultrafine eutectic spacing upon casting through proper selection of composition, alloying, and processing conditions. It is also increasingly realized that microstructures with variable length scale can yield unique properties, further expanding the domain of alloy development. For example, it is possible to take advantage of high strength and enhanced plasticity by designing the composite microstructure combining ultrafine or nanoscale eutectic matrix with micron-sized primary dendrites. It is also possible to achieve the right combination of strength and plasticity in the bimodal eutectic microstructure with heterogeneity in its length scale. Such bimodal eutectic microstructure can accommodate the localized strain. It has also been reported that the rotation of one eutectic colony with respect to another can dissipate the localized shear stress by the multiplication of shear bands. Therefore, the alloys with such microstructure show improvement in strength and plasticity (Fig. 3).

Various approaches and schools of thought exist regarding the simultaneous improvement in strength and plasticity in the eutectic alloys. The following can categorize these; i) control of volume fraction of primary dendrite phase, and number and type of dendrites including their nature (ordered or disordered), (ii) composite or heterogeneous microstructure where both coarse and fine eutectic microstructure is present, (iii) rotation of eutectic colonies with respect to each other. Recently, Tiwary et al. has demonstrated that a

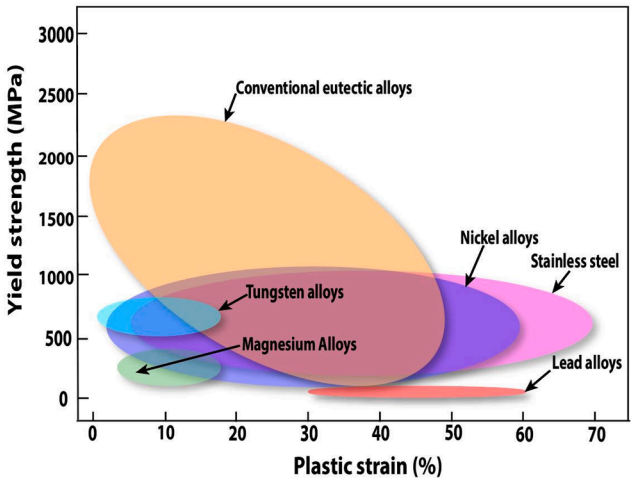

Fig. 3. Yield strength vs. plastic strain map for different structural alloys and eutectic alloys.

combination of different intermetallic results in a complex microstructure with a unique fractal dendritic growth morphology for Ni_3Al-Ni_7Zr_2 eutectic (Fig. 4). In the eutectic colony, they have observed a microstructural gradient with lamellar morphology at the initial stage that changes to rod and spiral morphologies during the thickening of the eutectic dendrite/colony [14].

In the subsequent sections, we shall briefly summarize the available information on eutectic alloys from the point of view of structural applications, followed by a discussion of the current trend and prospects. We have classified these in terms of systems that are suitable for applications in three specific temperature domains. These are domains of low-temperature applications represented by aluminum alloys, the mid-temperature domains exemplified by titanium and copper alloys, and the high-temperature domains represented by nickel-based superalloys and other similar alloys.

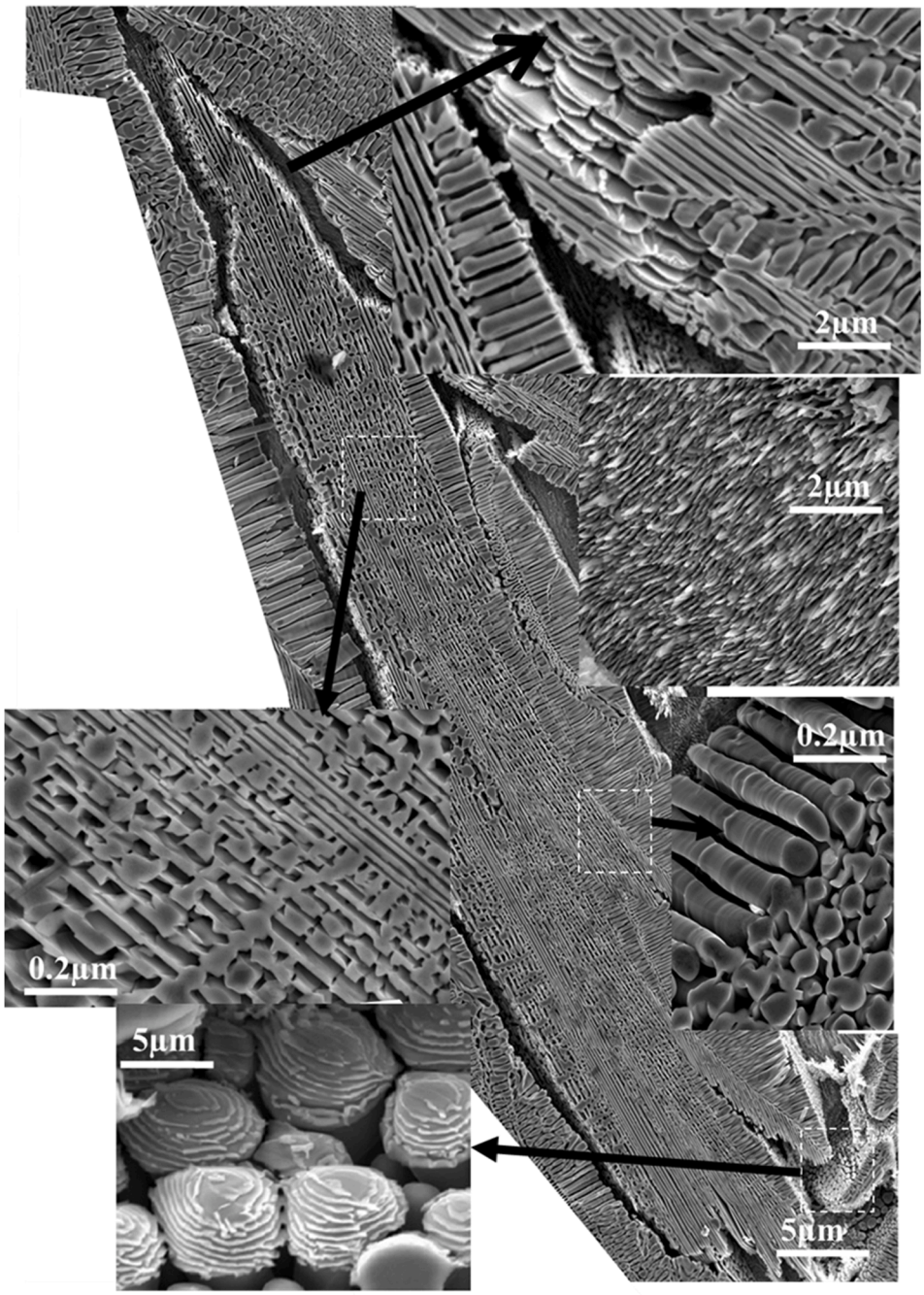

Fig. 4. SEM micrograph of an electro-etched complex eutectic alloy consisting of different morphology of eutectic lamellae [14].

2. Aluminum-based eutectic alloys

Aluminum (Al), the most abundant metal in the earth's crust, exists mainly in the form of bauxite in the earth. The low mass density of 2.70 g/cc, high oxidation resistance due to the formation of a thin protective layer of alumina (Al_2O_3), and high ductility due to more than five independent slip systems make it the most sought after structural materials for various structural applications. Due to these, aluminum (Al) and its alloys are up to 70% of the total content of automobiles' power trains, including engine, clutch, and various drive shafts. However, the ever-increasing demand to increase the engine's operating temperature for enhanced efficiency, reduced carbon emission, and increasing the strength and long-term sustainability at temperatures >473 K poses a major technological challenge for the application of cast Al alloys. The commercial age-hardened Al alloys show dissolution or coarsening of precipitates at high temperatures (>473 K). Therefore, to improve their high-temperature stability, additions of various transition elements such as Sc, Zr, Hf, V, and Ti have been carried out [15–19]. The addition of Zr and/or Sc in Al alloys helps maintain peak hardness during long-term exposure at 573 K. Additionally, Zr addition in Al-Sc alloys slows the precipitate coarsening kinetics and gives rise to high-temperature strength. However, despite these advantages, the cost-effectiveness of Sc addition and small volume fraction of the precipitates due to their limited solubility restricts their effectiveness as a high-temperature engineering material. Further, long-term exposure at temperatures beyond 673 K results in an escalated coarsening and formation of stable phases that are incoherent with the

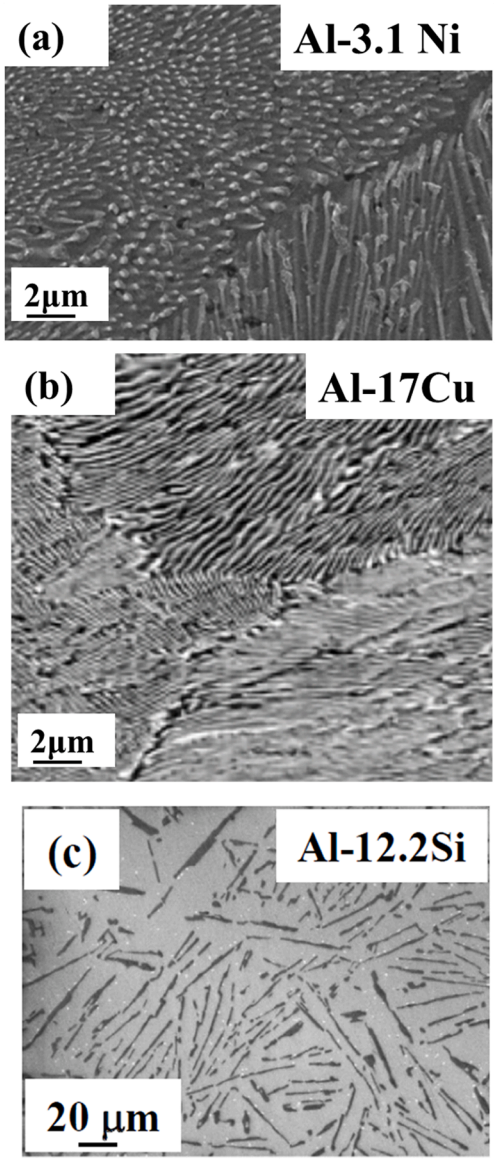

Fig. 5. Back scattered SEM micrographs of (a) Al-3.1Ni, (b) Al-17Cu and (c) Al-12.2Si eutectic alloys showing different eutectic morphologies [23,35].

matrix and therefore results in inferior mechanical properties. Developing castable eutectic alloys with good high-temperature mechanical properties, in this context, is attractive. Amongst all Al-based eutectics, Al-Al_3Ni (Al_3Ni rods in α-Al matrix), Al-Al_2Cu (lamellae or plates of Al_2Cu in α-Al matrix) and Al-Si (Si flakes in α-Al have drawn special attention [1–3]. These eutectic alloys show good strength at room temperature [2,3,20,21] due to the presence of a composite structure of hard Al_3Ni (orthorhombic crystal structure, Pnma), Al_2Cu (body-centered tetragonal, I4/mcm), and Si (diamond cubic, $Fd\bar{3}m$) phases in soft α-Al matrix (Fig. 5a-c) [22,23]. However, these alloys show poor stability at temperatures exceeding 473 K, which makes them unsuitable for high-temperature engineering applications. The poor microstructural stability in eutectics containing Al_3Ni rods is due to the presence of two kinds of instabilities at high temperatures: (1) morphological instability or spheroidization of rods and (2) size instability or breaking of rods [24]. During the solidification process, the formation of faults has been the major cause for instabilities, leading to the coarsening of the microstructural length scale [24,25]. Smartt *et al.* have reported that the coarsening of Al_3Ni rods follows the Ostwald ripening based on LSW coarsening mechanism where precipitate size (r) and time (t) follow the relationship $r^3 = k \times t$, where k is the coarsening rate [26]. The increase in average rod size and a concomitant decrease in number density leads to increased spacing between the rods and degrades the mechanical properties. Al-Al_2Cu eutectic shows a higher strength but poor plasticity due to the large volume fraction of hard Al_2Cu lamellae, which is incoherent with the α-Al matrix [27]. Similarly, Al-Si eutectic shows poor mechanical properties due to the weak interface between Al matrix and Si flakes [1]. However, the flake morphology of Si can be changed by small additions of modifiers such as strontium (Sr), sodium (Na), yttrium (Y), scandium (Sc), and/or suitable heat-treatment (T6 heat-treatment) [28–31]. These modifiers have led to an improvement in tensile properties, including plasticity [32,33]. However, Al-Si eutectics still suffer from poor elevated temperature performance. Ternary additions in the binary eutectics have been attempted to obtain bimodal/multimodal size distribution and form ternary eutectics with improved high-temperature mechanical properties. We will discuss some of these Al-based ternary eutectics and pseudo ternary eutectics in the successive sections, which may have future potential.

2.1. *Manipulation of mechanical properties of Al-Cu eutectic using length scale*

A quantitative relationship between lamellar spacing λ and solidification parameters such as V, G, and GV in Al-Cu alloys through the directional solidification process has been established. By adopting laser re-melting rapid solidification techniques, a detailed study of microstructure as a function of fundamental solidification parameters in Al-Cu eutectic alloy has been reported [34]. The experiments were performed on Al-17.1 at. % Cu (Al-32.7 wt% Cu) eutectic at speeds between 0.2 and 8 m/s. The microstructures were characterized by transmission electron microscopes followed by comparison with the available analytical model for eutectic growth under rapid solidification conditions. They found that at the interface between the laser trace and the non-treated base material, the re-solidifying eutectic bundle branches out from the coarse $A1_2Cu$ (Θ) phase present at the substrate. Only after a few microns., these lamellae grow parallel to the heat flow direction, reflecting a rapid increase in growth rate over a few microns. A wavy nature of the eutectic lamellae was observed at a solidification rate of about 20 cm/s. The observed nature of the eutectic growth between α-Al and Θ phases suggests a metastable eutectic growth. Recent studies reveal significant improvement in Al-Cu eutectic alloys' ductility with the refinement of microstructure (interlamellar spacing) [21,35]. Such refinements as reflected in the reduced interphase spacing (or interlamellar spacing for regular eutectic) can be affected by rapid solidification or alloying additions. Tiwary *et al.* developed Al-Al_2Cu eutectic with fine spacings (<1 μm) by suction casting the melt in a copper mold that leads to an order or two magnitude increase in strength (Fig. 6a) [35]. They also developed a quantitative model based on the interaction energy of the interfaces to predict the effect of length scale on the deformation process in the eutectics (Fig. 6b).

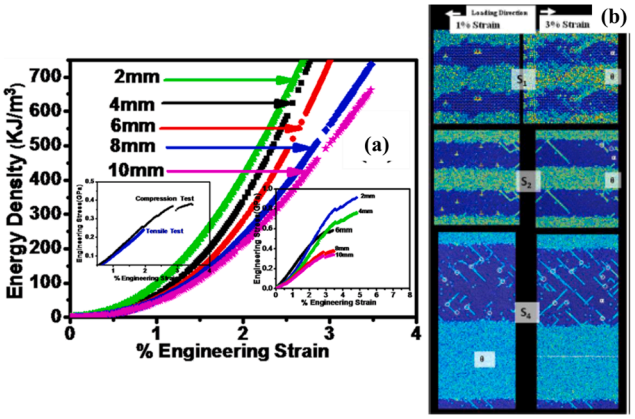

Fig. 6. (a) Energy density vs. percentage strain for different lamellar spacing. Inset: Experimental plot of engineering stress vs. percentage strain for different lamellar spacing during tensile and compression test. (b) The snapshot of MD (molecular dynamics) simulations of three lamellar spacing (6, 20, and 150 nm) at strains of 1 and 3%, showing different dislocation actively. Color coding was done based on Centro-symmetry [21,35].

2.2. Microstructure and mechanical properties of Al-based ternary eutectics

The microstructure and mechanical properties of the Al-Cu eutectic alloy can be further improved through ternary additions. Many studies are available on ternary eutectics and pseudo ternary eutectics (a combination of two binary eutectics with different morphology and length scale) with improved mechanical properties compared to their binary counterparts for high-temperature structural applications. The typical examples of such eutectics in ternary alloy systems are Al-Cu-Si and Al-Ag-Cu systems [36–38]. The Al-Cu-Si system showed two binary eutectics: non-faceted/non-faceted (nf-nf) Al-Cu and faceted/non-faceted (f-nf) Al-Si [36]. In comparison, two regular binary eutectics (nf-nf) and a ternary semi-regular brick type eutectic were reported in the Al-Ag-Cu system [38,39]. The richness of these microstructures has motivated attempts to design new ternary eutectic alloys. In the following section, we will discuss the microstructure evolution and its consequent effect on mechanical properties in ternary eutectic alloys of Al-Ni-X (X = Cr and Fe) and Al-Cu-Y (Y = Si and Ni).

2.2.1. Development of Al-Ni-Cr ternary eutectic alloys

The liquidus projection in the Al-Ni-Cr system was thermodynamically assessed by Huang *et al.* [40]. The phase evolution during solidification in the Al-rich portion was first experimentally studied by Compton *et al.* [41] and later by Pandey *et al.* [22]. Alloys studied by Pandey et al. exhibit composite microstructures that contain the A_3Ni phase embedded in α-Al matrix [22]. The Cr addition does not lead to any new phase formation. However, it does change the morphology and length scale of the eutectics. All ternary alloy compositions exhibit a core-shell architecture, with the Al_3Ni phase having a rod morphology in the core. At the same time, the rejection of Cr induces not only a cellular structure but also a lamellae morphology at the shell. The morphological instability-induced transition from lamellae to the rod is well reported in the literature [6,7,42]. However, such a transition in the same colony was noted by Pandey *et al.* [22] (Fig. 7a). The large buildup of Cr at the boundary layer led to a lower growth rate, which coincided with the Al_3Ni phase's morphological transition from rod to lamellae (Fig. 7a-c). Rosell-Laclau *et al.* reported that ternary eutectic composition Al-

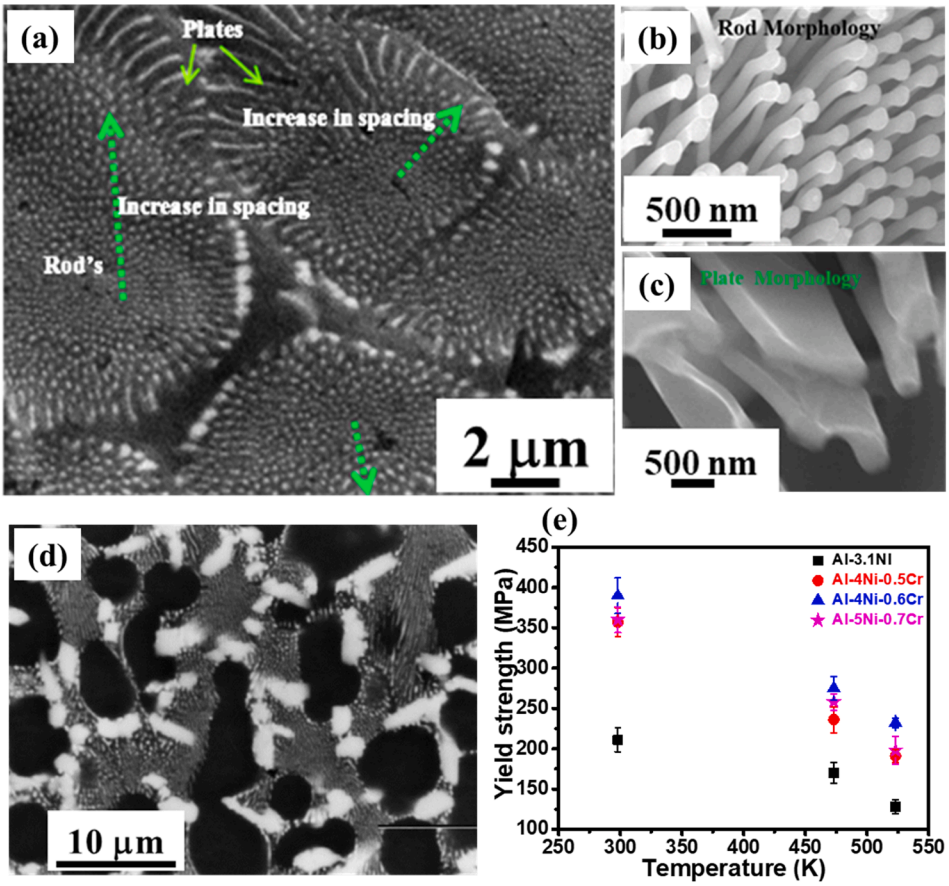

Fig. 7. (a) Backscattered SEM image of the suction cast Al-4Ni-0.6Cr alloy, revealing dual morphologies with an increase in eutectic spacing from center to colony boundary. (b) and (c) SEM images using a TLD (through the lens) detector elucidating dual morphologies, namely rods and plates, present in the eutectic colonies and at colony boundaries [22]. (d) Backscattered electron SEM micrograph of cast Al-2Ni-2Cr alloy, showing Al-Al_3Ni eutectic feature with bright Al_7Cr phase [41]. (e) Yield strength vs. temperature plot for Al-3.1Ni, Al-4Ni-0.5Cr, Al-4Ni-0.6Cr, and Al-5Ni-0.7Cr alloys [22].

2.9Ni-0.3Cr showed a eutectic reaction that results in the formation of α-Al + θ-Al_7Cr + Al_3Ni from the liquid phase at a univariant temperature of 908 K [43]. Compton. *et al.* experimentally studied the Al-rich portion of the Al-Ni-Cr phase diagram [41] with the Cr content of 2 at.% and beyond. The alloy with 2 at. % Ni and Cr showed a eutectic between Al and Al_3Ni phases along with the presence of irregular shape Al_7Cr phase (see Fig. 7d) [41]. Further addition of 5 at.% Cr in Al-2.0Ni alloy led to the formation of $Al_{11}Cr_2$ phase apart from Al_7Cr, Al_3Ni, and αAl phases leading to a complex phase equilibrium at 973 and 1273 K [44,45].

Binary Al-3.1Ni alloy under as-cast condition exhibits a hardness of 70 ± 4 HV [22]. Compton *et al.* reported an HV of 70 ± 3 for ternary Al-2.0Ni-2.0Cr alloy [41]. The HV increased to 128 ± 7 for Al-4Ni-0.6Cr. with increasing Ni, while HV of Al-6.0Ni-4.0Cr alloy was measured to be 151 ± 7. The hardness values of these alloys depend on the hardness of the intermetallic phase and its volume fraction, with the value decreasing in Al_7Cr, $Al_{11}Cr_2$, Al_3Ni, and αAl. Fig. 7e compares the yield strength values of binary Al-3.1Ni and ternary Al-4.0Ni-0.5Cr, Al-4.0Ni-0.6Cr, and Al-5.0Ni-0.7Cr alloys at room temperature, 473 and 523 K. The increment in yield strength in ternary alloys was 1.5 to 2 fold compared to the binary counterpart. For Al-4.0Ni-0.6Cr alloy, the maximum values of yield strength observed were 390 ± 22 MPa at room temperature 298 K), 275 ± 15 MPa at 473 K and 232 ± 6 MPa at 523 K. The higher yield strengths were attributed to the complexity of the hierarchical microstructure of the eutectics. The presence of core–shell type microstructure, particularly the lamellae structure at the colony boundary, has improved the fracture strain. The combined presence of two morphologies (rod and lamellae) can interact synergistically to delay crack propagation and improve plasticity [22].

2.2.2. *Development of Al-Ni-Fe ternary eutectic alloy*

The first experimental study on the Al-rich portion of the Al-Ni-Fe system was carried out by Premkumar *et al.* [46]. Rapid solidification of a set of three ternary alloys, Al-1.9Ni-2.1Fe (Al-3.9Ni-4.2Fe, in wt.%), Al-2.3Ni-2.5Fe (Al-4.8Ni 4.9Fe, in wt.%) and Al-

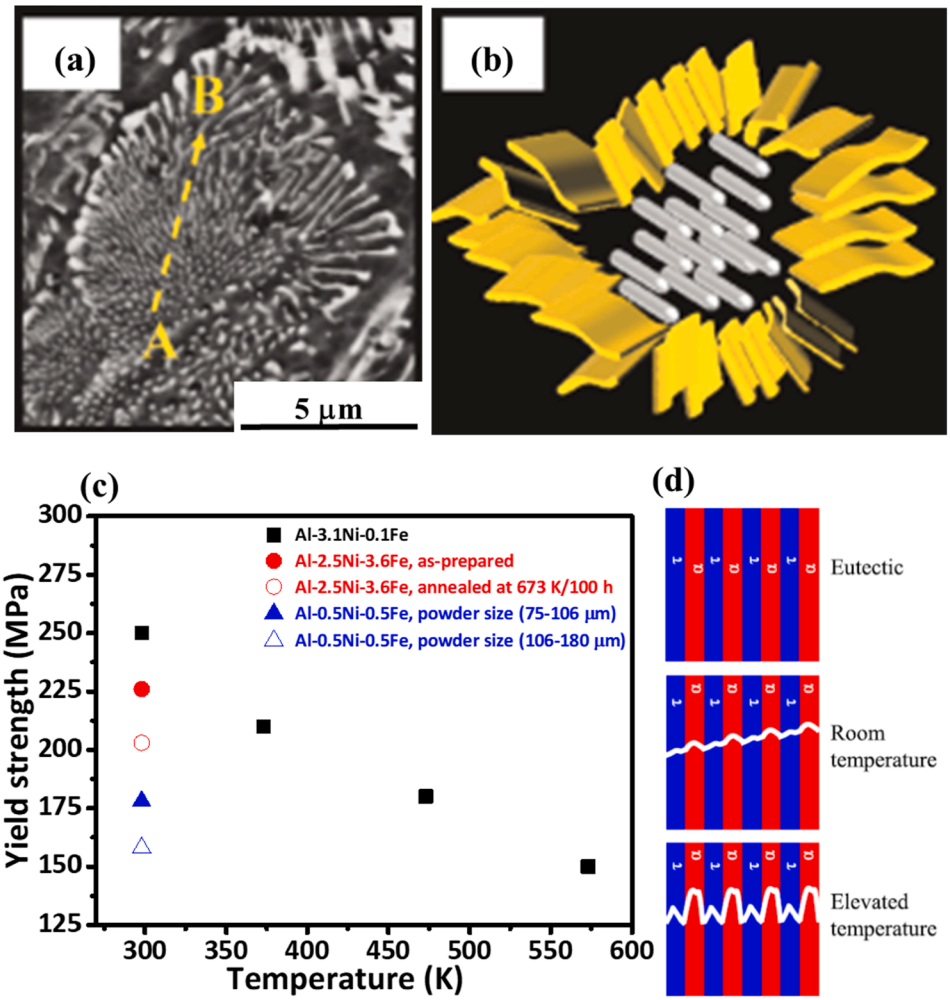

Fig. 8. (a) Backscattered SEM micrograph of the Al-3.1Ni-0.1Fe alloy revealing a eutectic colony with rod morphology at the center and lamellae morphology at the boundary [48]. (b) A Schematic showing dual morphology of the eutectic. (c) Yield strength vs. temperature plot for various Al-Ni-Fe alloys [48–50]. (d) A schematic depicting deformation of the eutectic during deformation under compression at room temperature and elevated temperatures.

2.9Ni-3.0Fe (Al-6.0Ni-5.9Fe, in wt.%) revealed microstructure with dual length scale involving the intermetallic phase Al_9NiFe. Fine-scale features observed consist of three morphologies: a fine intermetallic precipitate with a spherical/equiaxed morphology, a cellular matrix with the intermetallic phase at the cell walls, and lamellar eutectic microstructure with the alternate phase of α-Al and intermetallic phase. The coarser regions contained dispersoids of the intermetallic phase. A similar microstructure has also been reported in an atomized and compacted alloy of the ternary Al-Ni-Fe alloy. The ternary alloys exhibit good microstructure stability till 100 h at 673 K. A more detailed thermal stability study of an alloy Al-0.6Ni-0.9Fe at temperatures between 573 K and 898 K was reported by Bian *et al.* [47]. The coarsening studies at elevated temperatures show three different coarsening stages, with each stage having a different slope in the Ln(k) vs. temperature (T) plot. The first stage (573–673 K) represents the region with stable eutectic microstructure where the needle of Al_9NiFe showed a small increase in the diameter with no apparent increase in the length. The second stage (773–823 K) represents the transient coarsening stage where the eutectic phase experienced local ablation and coarsening and spheroidization of Al_9NiFe. At the third stage, the Al_9NiFe phase gets ruptured and spheroidized. The eutectic length scale increases rapidly at this stage. It was concluded that the shape change and bulk diffusion affected the spheroidization and coarsening process. A detailed study on the microstructural evolution and its effect on the mechanical properties of the suction cast alloy Al-3.1Ni-0.1Fe was carried out by Tiwary *et al.* [48]. Contrary to the observations mentioned earlier, the suction cast Al-3.1Ni-0.1Fe alloy showed a unique composite microstructure containing rod eutectic surrounded by lamellar eutectic (Fig. 8a). The microstructure also revealed a bimodal size distribution with fine rod eutectic(spacing ~90 nm) and a comparatively coarse lamellar eutectic (spacing ~140 nm). Fig. 8b shows the schematic of the eutectic colony depicting dual morphology. The TEM studies showed rods of Al_3Ni phase embedded in the α-Al matrix. The lamellae phase belongs to the intermetallic Al_9NiFe. The complex microstructure was rationalized by invoking an initial eutectic growth between Al and Al_3Ni that led to rejection of Fe. This build-up of Fe eventually leads to the formation of eutectic lamellae between Al and Al_9NiFe surrounding the initial colony of rod eutectic.

The mechanical properties (compressive yield strength) of the alloys both at room temperature and at elevated temperatures were

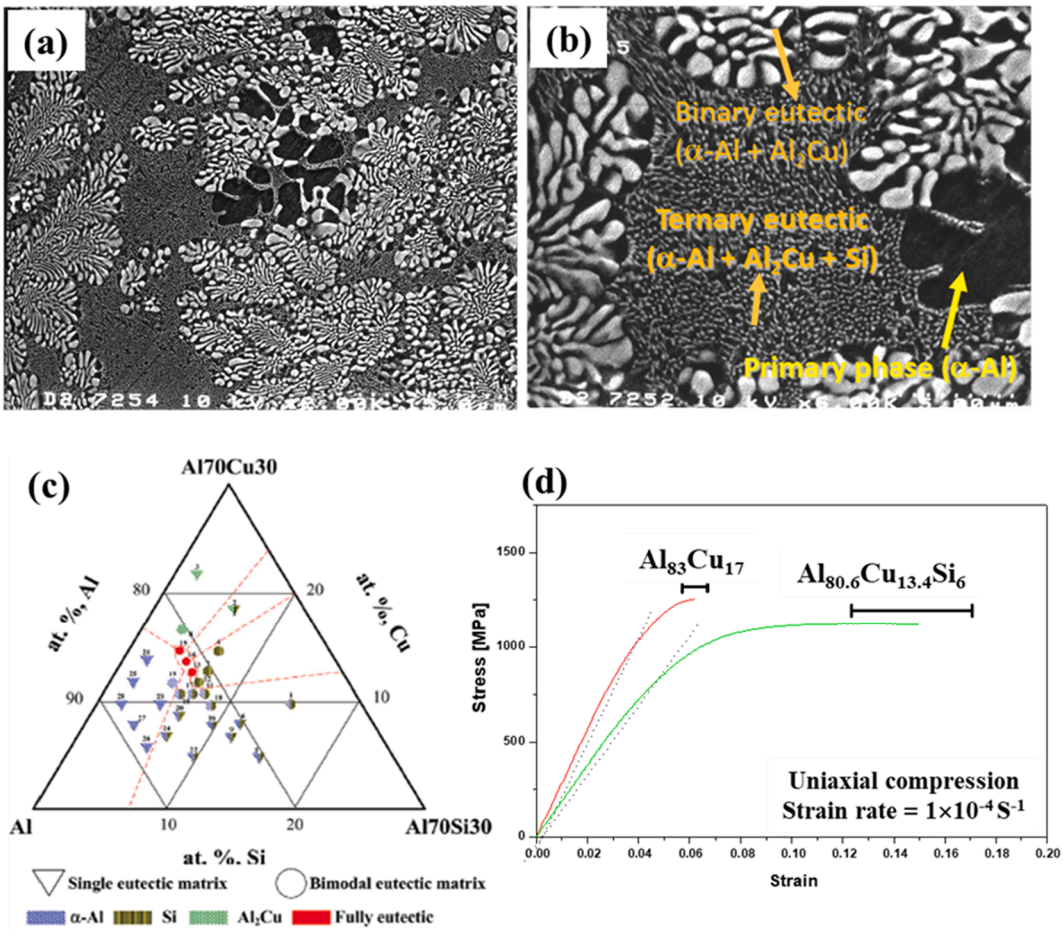

Fig. 9. (a) Backscattered SEM of the as-cast Al-13Cu-6Si alloy revealing the bimodal distribution of constituent phases. (b) High magnification SEM image of the Al-13Cu-6Si alloy. (c) Al-rich region of the Al-Cu-Si ternary phase diagram. The open circles represent compositions of the studied Al-Cu-Si ultrafine eutectic composite alloys [51]. Microstructural features observed in the various Al-Cu-Si alloys are shown via different symbols in the ternary Al-Cu-Si phase diagram. (d) Stress vs. strain plot for binary Al-Cu and ternary Al-Cu-Si alloys tested under compression.

summarized in Fig. 8c [48–50]. The Al-3.1Ni-0.1Fe alloy exhibits good strength till 573 K with a yield strength of 250 MPa at room temperature. Increasing the temperature to 573 K leads to a decrease in strength to 150 MPa with a consequent increase in compressive plasticity. This improvement in properties was attributed to the bimodal size distribution of rod and lamellae eutectic between the hard intermetallics of Al_3Ni and Al_9NiFe phases. The smaller size of colony and refinement of eutectic can result in a large accommodation of plastic strain at the colony boundaries that gives rise to good plasticity.

Additionally, the colony boundaries also can affect the crack path during deformation. However, the necking of the Al_3Ni phase was observed at higher temperatures due to an increase in plasticity. The fracture surface at 573 K revealed the breaking of Al_3Ni rods while the Al_9NiFe phase retained its shape with the formation of voids around it, suggesting that it had resisted the deformation locally. The yield strengths of alloy Al-2.5Ni-3.6Fe in the as-prepared and annealed condition (at 673 K for 100 h) were reported to be 226 and 203 MPa, respectively [49]. This small drop in strength after long-term aging indicates good microstructural stability of the eutectic microstructure. On the other hand, the atomized, compacted, and extruded powders of compositions Al-0.5Ni-0.5Fe showed yield strength of 178 and 158 MPa for the powder size ranges of 75–106 and 106–180 μm, respectively [50].

2.2.3. Development of Al-Cu-Si eutectic alloys

An in-situ grown bimodal ultrafine eutectic composite microstructure in Al-based alloys was first reported by Park *et al.* [36]. This report introduced the nanoscale composite with hierarchy in the length scale in an Al-13Cu-6Si alloy by carefully controlling the solidification parameters. Compared to the binary Al-17Cu eutectic alloy that showed lamellar morphology between αAl and Al_2Cu phases, the ternary eutectic exhibits a bimodal distribution of constituent phases and heterogeneity in the length scale (Fig. 9a, b). The microstructure contains micron size (10–20 μm) cellular colony of eutectic of α-Al and θ-Al_2Cu having the interlamellar spacing of 300 to 700 nm and regions having a complex nanostructured ternary eutectic containing three different phases α-Al, Si, and Al_2Cu. A change in composition with reduction of copper content introduces primary dendrites of α-Al along with the ternary eutectic. Kim *et al.* studied a swath of composition space in the Al-rich corner of the Al-Cu-Si system for establishing the role of different microstructural characteristics such as length scale and phase volume fraction on mechanical properties [51]. The compositions and the microstructural features are marked in the Al-Cu-Si phase diagram (Fig. 9c). The Ni addition of 3 and 5 at. % of Ni by replacing Cu in the Al-13Cu-6Si alloy resulted in the formation of the primary dendrites of Al_3Ni_2 embedded in a α-Al and nanostructured eutectic of α-Al +

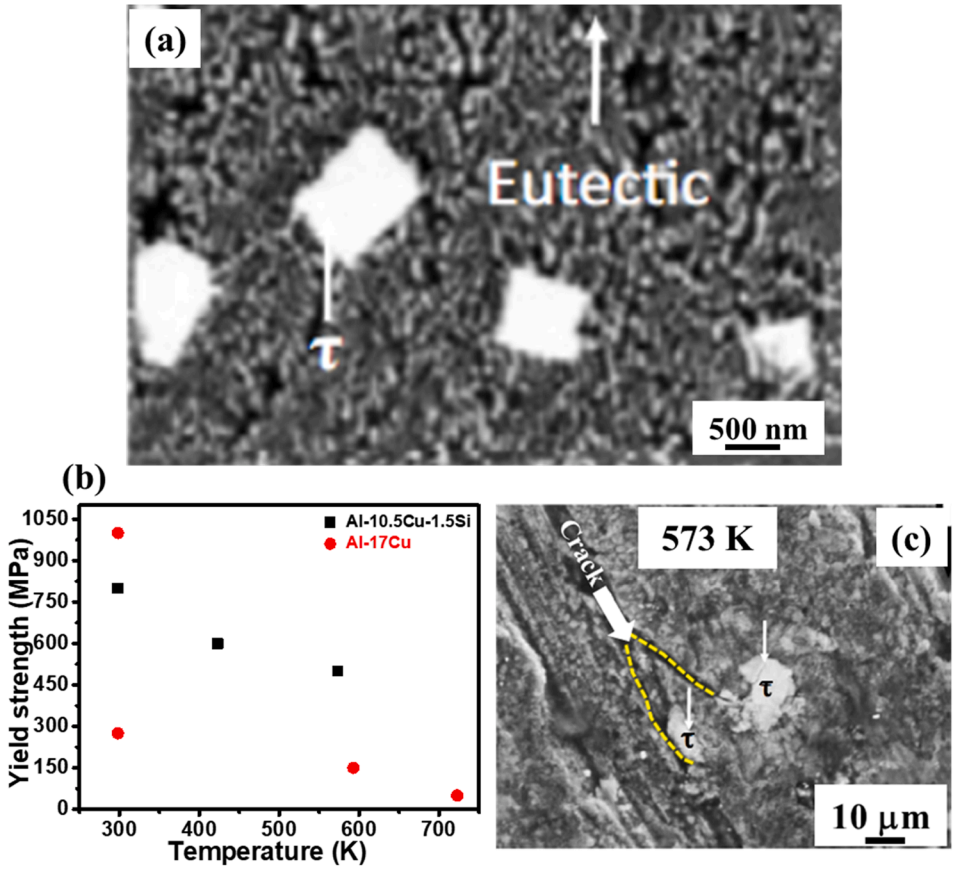

Fig. 10. (a) Backscattered SEM image of the suction-cast Al-10.5Cu-1.5Ni alloy. (b) Yield strength vs. temperature plot for the suction cast Al-10.5Cu-1.5Ni alloy and its comparison with the binary Al-Cu alloy [2,27,36]. (c) Secondary electron SEM micrographs of the fracture surface of Al-10.5Cu-1.5Ni alloy deformed at 573 K.

Al_2Cu + Si [52]. Ramakrishnan *et al.* studied the effect of varying cooling rates in the Al-13Cu-6Si alloy by employing laser surface remelting [53]. In this study, the cooling rate has significantly affected the solidification microstructure, phase morphology, and distribution. With the cooling rate greater than 4.03×10^4 K/s, the ultrafine ternary eutectic disappears and is replaced by the binary α-Al + Si eutectic. Thus the microstructure consisted of dual-binary eutectic: α-Al + Al_2Cu and α-Al + Si.

The Al-13Cu-6Si eutectic nanocomposite with hierarchical length scale exhibits an excellent combination of yield strength (800 ± 50 MPa), ultimate fracture strength (1100 ± 100 MPa), and plastic strain (11 ± 2%) at room temperature [36]. A comparative stress–strain diagram of ternary eutectic with binary Al-Cu eutectic is shown in Fig. 9d. The excellent combination of properties was attributed to the uniform distribution of the multiple shear bands throughout the deformed sample, releasing the highly localized shear deformation, suppressing crack propagation. The improvement in strength can be related to a Hall-Petch type strengthening. The refinement of eutectic resulted in increased strength. The detailed TEM study of the deformed Al-9Cu-6Si alloy (up to 8%) showed the presence of dislocation activities in the ductile α-dendrites with the formation of dislocations networks at the dendrite and nanostructured ternary eutectic boundaries [54]. It implied that the deformation of α-Al dendrites occurs by a dislocation slip mechanism. However, the brittle Al_2Cu phase's deformation is accompanied by shear bands, which are arrested at the ductile α-Al boundary. Nano cracks could not be observed until the plastic deformation reaches up to 25%, confirming that large plastic strain was realized due to simultaneous shear and slip band formation.

2.2.4. Development of Al-Cu-Ni eutectic alloys

Tiwary *et al.* studied the phase evolution in the cast Al-Cu-Ni near eutectic alloys that exhibit complex microstructure containing eutectics that significantly influence the mechanical properties [27]. For an alloy Al-10.5Cu-1.5Ni, the microstructure consists of a faceted primary phase of τ-Al_7Cu_4Ni coexisting with fine eutectic of α-Al and θ-Al_2Cu (Fig. 10a). Maity *et al.* studied the phase evolution in the cast alloys with a slightly higher Cu and Ni [55]. In these alloys, both α-Al and vacancy ordered phase Al_3Ni_2 coexists as a primary phase with a fine lamellar eutectic between α-Al and Al_2Cu. Thus, these alloys exhibited a bimodal distribution with micron-size primary α-Al and vacancy ordered phase (VOP) and nanoscale lamellar eutectic. The following is the phase formation sequence:

$$L \rightarrow VOP + L_1 \rightarrow VOP + \alpha - Al + L_2 \rightarrow VOP + \alpha - Al + (\alpha - Al + \theta - Al_2Cu)_{eutectic}$$

Fig. 10b shows a comparison of temperature-dependent yield strength of Al-10.5Cu-1.5Ni and Al-17Cu alloys [2,27,36]. Although the room temperature strength of binary eutectic is higher than the ternary eutectic, the bimodal distributed ternary eutectic alloy showed better strength between 373 and 573 K. However, the room temperature yield strength of 1000 MPa for binary alloy, as reported by Park *et al.* [36], is higher than that of 275 MPa for the same alloy, reported by Cantor et al. [2] and 800 MPa for the Al-10.5Cu-1.5Ni alloy. The bimodal eutectic showed a plastic strain of 9% higher than the plastic strain of 2% for Al-17Cu alloy [27,36]. This large difference in plastic strain was rationalized by studying the fracture surface of the deformed alloys. The fracture surface of room temperature deformed Al-10.5Cu-1.5Ni alloy showed uniform shear band formation throughout the sample. The bimodal nature of eutectic in ternary alloy helped delay the localized shear deformation. The micron-size ternary Al_7Cu_4Ni phase that coexists helps divert the crack propagation path or hinder the crack propagation, especially at high temperatures (Fig. 10c).

2.3. Comparison of mechanical properties of different Al alloys

Fig. 11a presents the room temperature yield strength vs. ductility plot of ternary eutectic alloys that exhibit complex eutectic microstructure. Fig. 11b shows the variation of yield strength at room temperature as a function of eutectic spacing for alloys with the unimodal distribution as well as the bimodal distribution of eutectic with varying length scales of various Al alloy composites [19,22,27,29,36,48–50,52,54,56–66]. The length scale heterogeneity with the complex distribution of phases placed the bimodal eutectic in a better strength-ductility trade-off than the unimodal eutectic, and other precipitation hardened Al alloys. The bimodal and

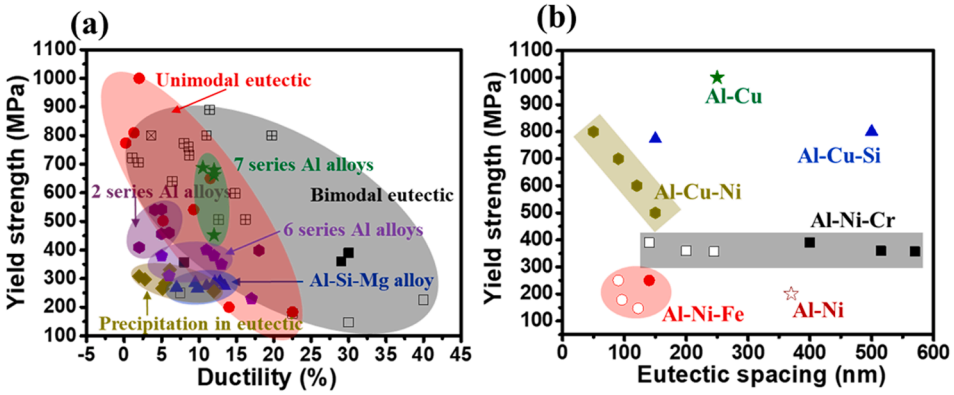

Fig. 11. (a) Yield strength vs. ductility plot for various developed Al-based alloys [1,19,22,27,29,36,48–52,54,56–66]. (b) Yield strength vs. eutectic spacing plot for binary and ternary Al-based eutectics. The open symbols represent rod spacing, whereas the close symbols represent lamellae spacing.

multimodal eutectic derived their strength through nano-structuring of the phases that leverage Hall-Petch strengthening and the strengthening mechanisms that consider the dislocation-based slip transfer and accommodation of shear through shear bands due to the complex distribution of phases in the microstructure of micron-sized eutectics [51,54]. In contrast, the unimodal binary eutectics such as Al-Al_2Cu, Al-Al_3Ni, and Al-Si and ternary eutectics Al-Ni-Fe, Al-Cu-Si showed either high strength or better compressive plasticity and hence, did not possess a superior strength-ductility trade-off [1,22,27,36,51]. The addition of transition elements such as V, Ti, Sc, Zr was attempted in recent times to improve the mechanical properties of Al eutectic alloys [55–57,60,64,67,68]. The effects were more pronounced at higher temperatures (<473 K). Mondol *et al.* reported that the addition of Sc and Zr to 2219 alloy increased the room temperature yield strength from 345 to 455 MPa with a reduction in tensile plasticity from 12 to 5% [56]. Similar effects due to transition metal additions were also observed in other Al alloys. The improved mechanical properties were attributed to the presence of coherent $L1_2$-Al_3X (where × = V, Ti, Sc, Zr) particles that showed better thermal stability. Following a similar concept, the mechanical properties of Al eutectics were enhanced by small additions of Zr and Sc that resulted in precipitation of fine (5–10 nm) $L1_2$ ordered precipitates in α-Al matrix. The Sc addition in an Al-Si eutectic alloy led to a significant increase in room temperature yield strength [29]. Suwanpreecha *et al.* observed that the precipitation of Al_3Sc nano precipitates in the soft α-Al matrix in α-Al-Al_3Ni eutectic resulted in a significant increase in yield strength at 573 K as well as a two-fold increase in the threshold stress during creep at the same temperature [68,69]. Pandey *et al.* reported that the addition of 0.15 at.% of Zr in Al-3.1 Ni alloy led to improved yield strength at room temperature and 523 K. Zr addition also provided microstructural stability during aging at 673 K due to segregation at the Al/Al_3Ni interface.

The yield strength of eutectics depends on three factors: eutectic spacing, colony size, and heterogeneity in the length scale (unimodal, bimodal, or multimodal). The yield strength dependency on the eutectic spacing (like grain size) follows the Hall-Petch type relationship, as was discussed earlier. While Tiwary *et al.* showed a logarithmic dependency between strength and lamellae spacing in Al-Al_2Cu eutectic [35], some other reports suggest an inverse dependency between them [70–72]. It was argued that the change in the exponent is related to the change in the deformation mechanism. The plot between yield strength vs. eutectic spacing (rod and lamellae) in various binary and ternary eutectic is shown in Fig. 11b. The refinement in Al-Cu-Ni and Al-Ni-Fe eutectic has increased the yield strength. However, despite the sizeable lamellar spacing, Al-Cu-Si alloys showed excellent mechanical properties due to bimodal size distribution.

3. Copper-based eutectic alloys

Although comparatively limited in numbers, copper possess several important eutectic reactions in combination with other elements from the periodic table. Many of them are characterized by significant free energy changes leading to a deep eutectic in the phase diagram. The many prominent eutectics of copper have low melting points, and hence they are at the forefront of the development of lead-free solders, including the Sn-Ag-Cu eutectic (SAC) solder alloys. These are reviewed extensively in the literature [73–78]. The second prominent development involving copper-based eutectic composition is in designing copper-based metallic glasses. The most prominent being Cu-Zr, these systems also exhibit deep eutectic, a primary requisite for the formation of metallic glass. Both these copper-based eutectic alloys have important engineering applications and are extensively reviewed [79–82]. However, the increasing demand for new alloys for high conductive and high-temperature applications has made the prospect of newer copper alloys, including eutectic alloys, attractive. This section will present a set of well-established binary and ternary copper-based eutectic systems and draw attention to few exciting and promising possibilities in the realm of alloy design for high strength and high conductivity applications.

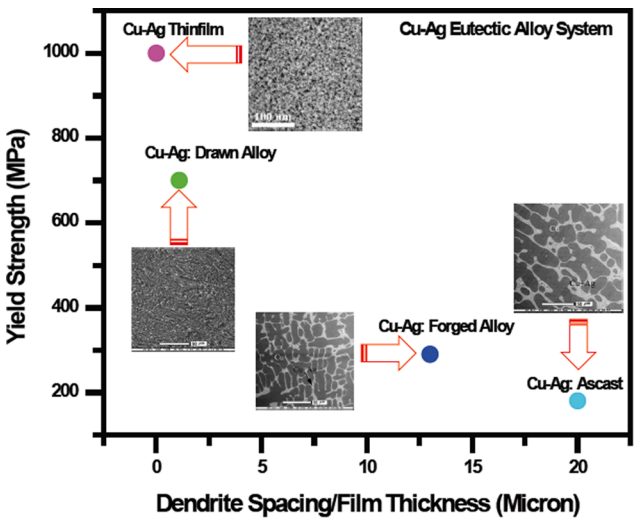

Fig. 12. Length scale vs. strength relation of different Cu-Ag Alloys [83–86].

Among all Cu-based eutectics, the Cu-Ag eutectic is one of the most studied alloys. In general, this eutectic exhibits a well-defined lamellar microstructure [83–86]. The eutectic, with higher undercooling or growth rate, displays a feathery lamellar morphology that coexists with dendritic or colony structure with a two-phase irregular eutectic morphology. Due to inherent high conductivity and the possibility of increasing the strength by reducing length scale, the Ag-Cu ultrafine eutectic alloys with varying amounts of primary dendrites of either copper or silver (depending on compositions) are attractive for high conductive high strength applications. The decrease in length is possible not only by controlling solidification conditions but also through mechanical processing like drawing [83] and through thin film deposition [85] that inherently produces a fine fibrous/lamellar eutectic structure. This feature yields a very high strength with good conductivity suitable for electrical applications. A summary of the mechanical properties of this alloy has been illustrated graphically in Fig. 12.

Copper also forms eutectic with a selection of copper-based intermetallics like Cu_2Mg [87] and Cu_3La [88]. Both eutectics are used for high conductivity applications that require good strength. One of the more popular copper-based eutectic systems is the Cu-Zr system, known for forming metallic glass. There are reports of two lamellar eutectics with Cu_5Zr and Cu_9Zr_2 intermetallic compounds [80]. The strength of these eutectic varies from 0.6 to 1 GPa while they have relatively low electrical conductivity. In terms of strength to conductivity performance, the eutectic in Cu-B systems provides one of the best performances with a reported strength of ~ 340 MPa with Electrical conductivity of 83% of IACS [89]. A potential and less studied eutectic is observed in binary Cu-Ge alloy. It may have potential use in large-scale integrated circuit technology. The eutectic in Cu-Ge alloy forms at 36.5 at.% Ge and contains a

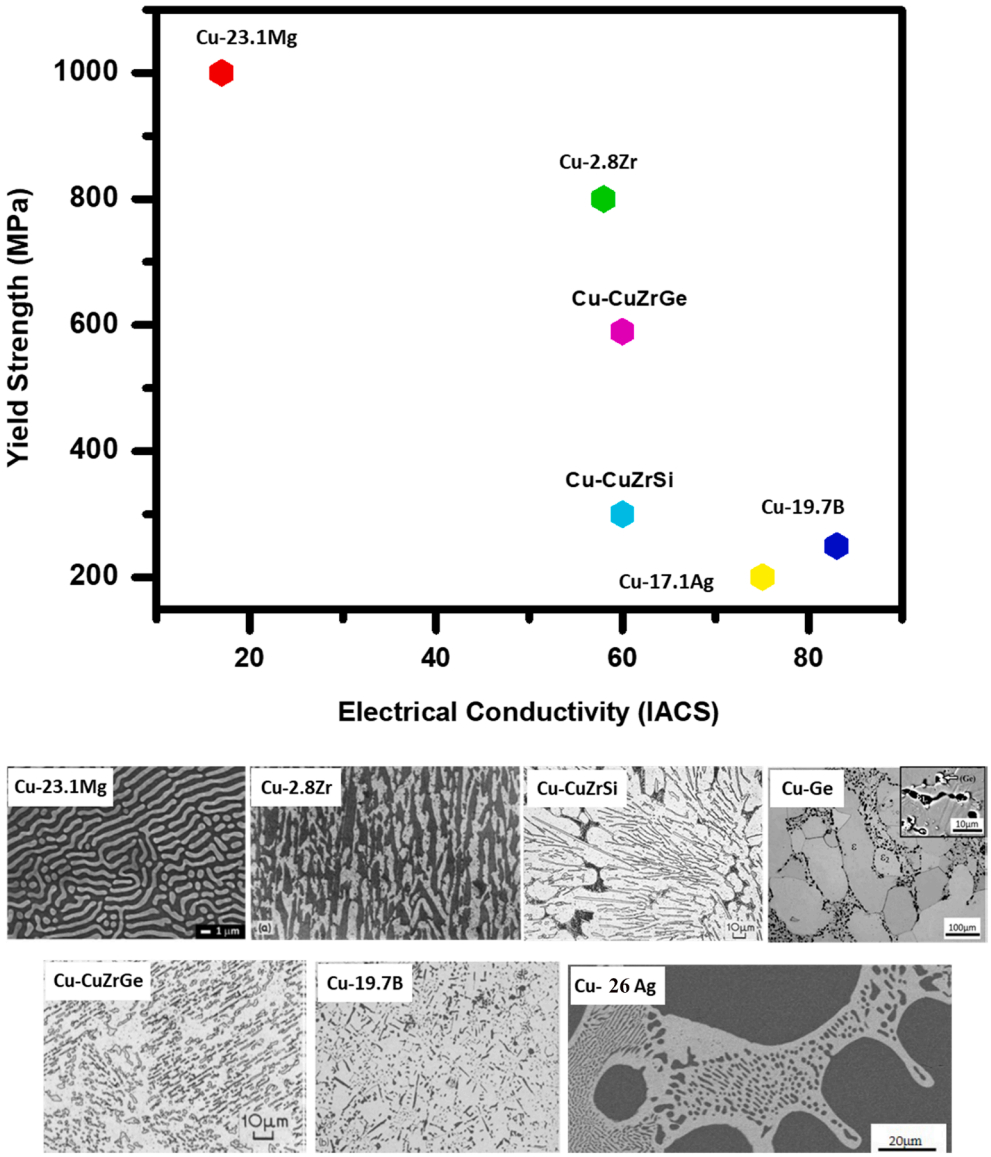

Fig. 13. Typical Microstructural Evolution in different eutectic copper alloys [80–82,87–93].

mixture of intermetallic ∈ and primary semiconducting Ge in their eutectic microstructure. The microstructure in this system can be tuned by solidifying it at different undercooling [90].

There are several studies on the formation and properties of eutectics in ternary copper base alloys. A very high strength (UTS of 1578 MPa) is observed in the ternary eutectic Cu-14 wt% Fe-3 wt% Ag (Cu-15.8 at.% Fe- 1.8 at.% Ag) where primary Fe rich phase coexist with very fine eutectic of Cu and Ag [91]. A ternary intermetallic phase $CuTi_3Sn_5$ is reported to form a eutectic with copper in a Cu-Ti-Sn system that yields a very high hardness [92]. Several copper-containing ternary eutectics have been explored for applications that demand both high-strength and high conductivity simultaneously. A broken lamellar eutectic has been reported in a directionally solidified Cu-CuZrSi pseudo-binary system with a maximum yield strength of the order of ~ 390 MPa while retaining the Electrical conductivity of 60% of IACS [81]. In the case of Ge replacing Si, the ternary eutectic of Cu-CuZrGe show a eutectic colony structure with an even higher strength of 450 MPa with identical conductivity [93]. A summary of the strength versus Electrical conductivity plot of different copper alloys is shown in Fig. 13.

4. Titanium-based eutectic alloys

Over the past few decades, titanium and titanium-based eutectic alloys have been studied extensively by both academic and

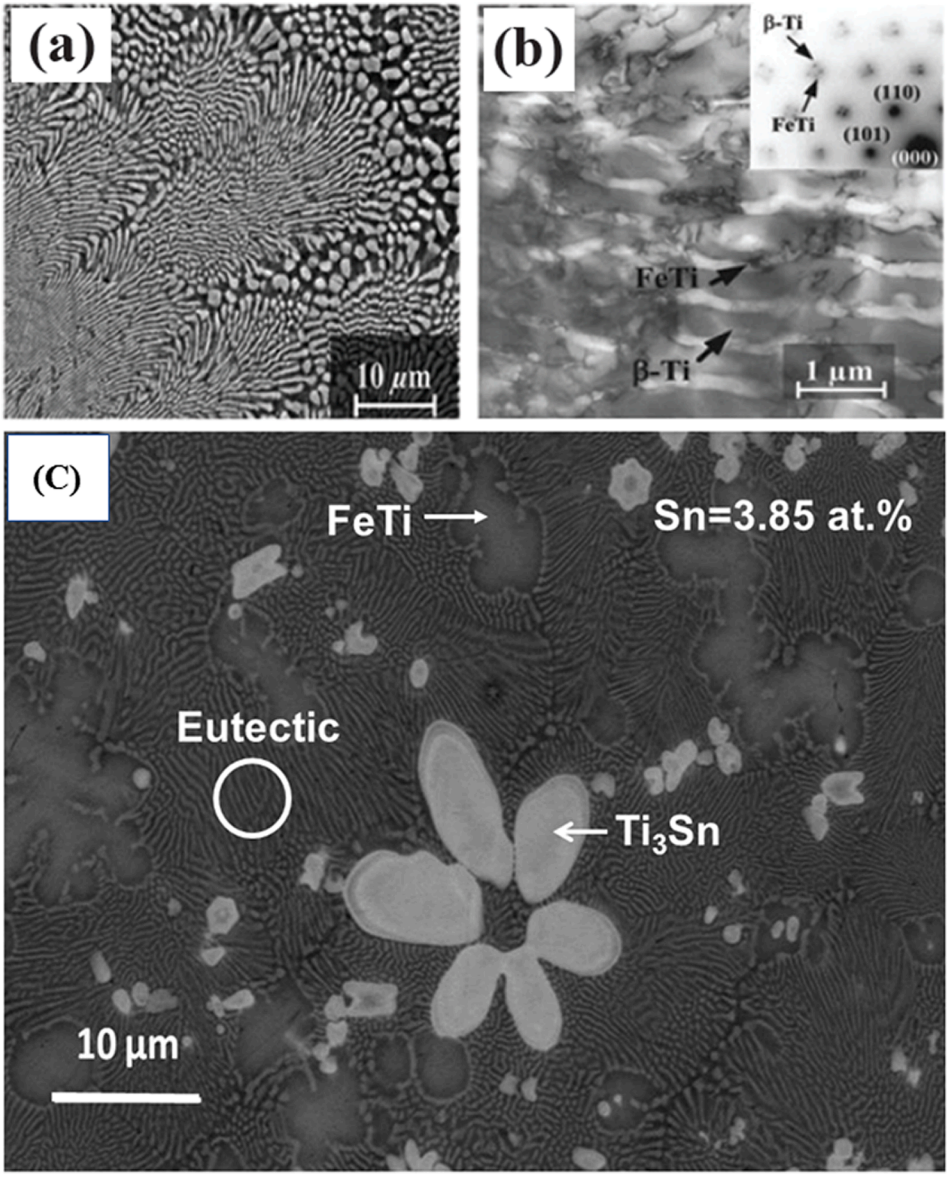

Fig. 14. SEM micrographs of as-cast cylinders: (a) $Ti_{67.79}Fe_{28.36}Sn_{3.85}$ alloy [103]; and corresponding TEM micrograph is shown in (b) [104]. (c) The SEM backscattered electron micrographs of $Ti_{71}Fe_{29-x}Sn_x$ (x = 3.85at. %) alloy [111].

technological community across the globe due to their superior properties, including a high strength to weight ratio due to the low density of titanium (4.5 g/cc), excellent corrosion resistance, improved fracture toughness, and ductility, good biocompatibility, and chemical stability [94]. The development of novel Ti-based eutectic alloys needs a design methodology, which is distinctly different from other alloy systems. The most extensively investigated Ti base eutectic alloys are obtained by alloying Fe with Ti [95,96]. In binary Ti-Fe systems, the eutectic point lies at a composition of 29.5 at.% Fe and temperature of 1358 K. The eutectic has a lamellar morphology, the scale of which can be altered by controlling the solidification parameters. The strength depends on the interlamellar spacing (Fig. 16a). Compared to the eutectic and hypoeutectic alloys, hyper eutectic alloys in the Ti-Fe system exhibit higher strength due to the FeTi primary phase's better strength. The maximum strength of 2.2 GPa with plasticity of 6.7% had been reported in these alloys [95]. A majority of the potential ternary eutectic alloys of Ti are based on the binary Ti-Fe alloy. The development leverages the better knowledge of the phase formation and microstructure evolution and is based on Ti-Fe-X where X represents Sn, Co, Mo, Ni, In, Nb, Ta, V, Zr, and Ga [97–102].

4.1. Development of Ti-Fe-Sn eutectic alloys

We shall first highlight the microstructure evolution and mechanical properties of multicomponent Ti-Fe-Sn ternary eutectic alloys. These are synthesized using arc melting followed by suction casting. The binary Ti-Fe eutectic ($Ti_{70.5}Fe_{29.5}$) is a biphasic eutectic containing (β-Ti) and TiFe (B2) intermetallic. The typical eutectic microstructure of $(Ti_{70.5}Fe_{29.5})_{100-x}$ Sn_x (x = 3.85) alloy (Fig. 14a, b) exhibits a cellular eutectic morphology of broken rods due to the addition of Sn to the binary Ti-Fe alloy [103,104]. Both the binary and ternary alloys exhibit identical orientation relationship between β-Ti phase and FeTi phase (i.e. $[110]_{\beta\text{-Ti}} \,||\, [110]_{FeTi}$ and $[199]_{\beta\text{-Ti}} \,||\, [199]_{FeTi}$) revealing good compatibility between the two phases in the eutectic matrix. However, the difference in lattice parameters between β-Ti and FeTi of the eutectic changes with the addition of Sn in Ti-Fe alloys. The microstructure consists of relatively ductile dendrites of (β-Ti) solid solution coexisting with large volume fractions of eutectic between (β-Ti) and TiFe or (β-Ti) and Ti_3Sn (Fig. 14c). μm-sized dendrites provide ductility and toughness, whereas ultrafine/nanoscale eutectic provides superior strength. However, a possibility exists for the formation of a three-phase eutectic ((β-Fe), TiFe, and Ti_3Sn) or a bimodal distribution of different eutectic colonies to bring about novelty in the microstructure. These are often achieved by adopting various processing routes along with variations in alloy compositions. The solidification behavior of suction cast Ti-Fe-Sn alloys with a systematic variation of Sn has been studied to understand the evolution and morphologies of constituent phases [105–109]. The variation of yield strength and plastic strain as a function of different interlamellar spacings in Ti-Fe-Sn eutectic is shown in Fig. 16c.

A bimodal eutectic structure was observed by Han *et al.* [105,110] during solidification. It is explained using 'ternary quasi-peritectic' equilibria involving four phases, Ti_3Sn, L, FeTi, and β-Ti. The ternary quasi-peritectic' reaction L + Ti_3Sn → β-Ti + FeTi is coupled with two univariant reactions (i) L → β-Ti + FeTi and (ii) L → β-Ti + Ti_3Sn. Samal *et al.* [111], in their investigation on $Ti_{71}Fe_{29-x}Sn_x$ (x = 1 to 10 at.%), presented the evidence of peritectic reaction responsible for the formation of intermetallics that coexist with eutectics and dendrites, leading to a complex microstructure. Das *et al.* [104], in a detailed study of $(Ti_{70.5}Fe_{29.5})_{100-x}Sn_x$ (with × = 0, 3.85) alloys, reported very high strength (2260 MPa) with sufficient ductility (9.6%) compared to Ti-Fe binary alloy with strength ∽ 1935 MPa and ductility of 2.6%. It is attributed to the variation in eutectic morphology and the distribution of the intermetallic FeTi phase. A good combination of high ultimate strength (∽1718 MPa) and plasticity (∽ 12.8%) was also reported by Mondal *et al.* [112] in the $Ti_{71}Fe_{25.15}Sn_{3.85}$ alloy. It can be compared to the $Ti_{71}Fe_{29}$ binary alloy (ultimate strength ∽ 701 MPa and plasticity ∽ 3.8%). The presence of two eutectics at different length scales is responsible for this improvement.

4.2. Ti-Fe-Co multicomponent eutectic alloys

The ternary addition of Co to the binary Ti-Fe eutectic alloys also leads to a refinement of the lamellae with the formation of

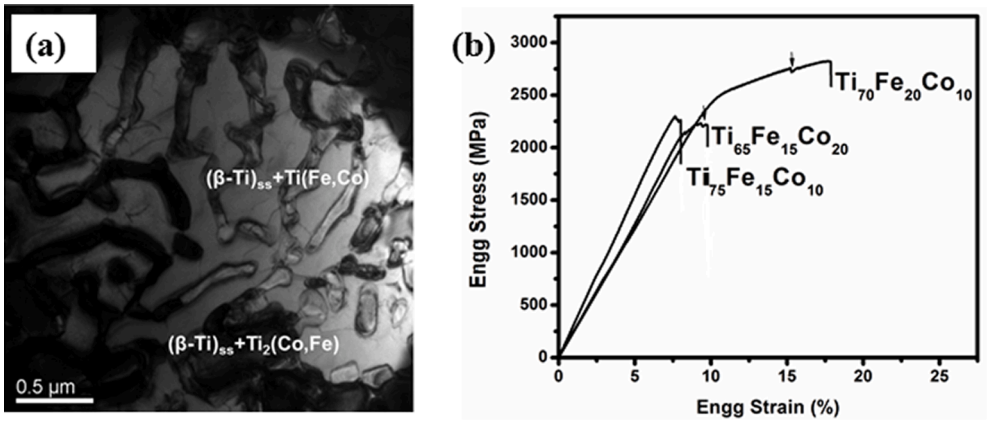

Fig. 15. (a) Bright-field micrograph showing bimodal eutectic microstructure, (b) Room temperature compressive engineering stress-strain curves of Ti-Fe-Co alloys [118].

intermetallic/intermediate compounds (TiFe ($Pm\bar{3}m$, a = 0.2975 nm), TiCo ($Pm\bar{3}m$) and Ti_2Co ($Fd\bar{3}m$, a = 1.129 nm)). The element Co, having a higher melting temperature than Sn, increases these ternary alloys application temperature with a slight increase in the density (5.6 g/cc). The presence of several intermediate phases in this system offers various possible pathways to design and develop novel microstructures with simultaneous improvement of mechanical properties at room and high temperatures [113–116]. Samal *et al.* [117] reported the microstructural evolution of a series of hypoeutectic $Ti_{75}Fe_{25-x}Co_x$ (0, 5, 10, 12.5, 15, 20), eutectic $(Ti_{70.5}Fe_{29.5})_{100-x}Co_x$ (x = 0, 2, 4, 6, 8 and 10), hyper eutectic $Ti_{70}Fe_{30-x}Co_x$ (x = 0, 5, 10, 15, 20, 25), $Ti_{65}Fe_{35-x}Co_x$ (0, 10, 15, 17.5, 20, 25) and $Ti_{60}Fe_{40-x}Co_x$ (x = 0, 16, 18, 20, 22, 24) alloys. The $Ti_{70}Fe_{20}Co_{10}$ alloy exhibits unique microstructural features consisting of two eutectics at different length scales. The typical microstructure of $Ti_{70}Fe_{20}Co_{10}$ alloy (Fig. 15a) shows the evolution of two eutectics through the reactions L → $(\beta\text{-Ti})_{ss}$ + Ti(Fe, Co) and L → $(\beta\text{-Ti})_{ss}$ + Ti_2(Co, Fe). As Ti2(Co, Fe) formation is pivotal for the microstructural evolution in the Ti-Fe-Co alloys, the solidification pathways can be understood by generating liquidus surface projection on the Gibbs triangle plot of Ti-Fe-Co alloys [117]. Samal *et al.* [118] reported mechanical properties of a series of Ti-Fe-Co alloys (shown in Fig. 15b). $Ti_{70}Fe_{20}Co_{10}$ alloy consisting of bimodal eutectics shows the well-balanced mechanical properties (i.e., strength ~ 2819 MPa and plasticity ~ 8.5%) among the series. Further alloying additions in Ti-Fe-Sn and Ti-Fe-Co can improve the properties of this class of alloys. An ultrafine eutectic structure with 1.1 GPa strength and 11% ductility is recently reported in a quinary Ti-16.6Nb-6Co-5.1Cu-6.5Al (at%) [119].

4.3. Ti-Fe-X ternary and quaternary eutectics

The addition of Zr in the Ti-Fe system yields various Laves phases forming eutectics with β-Ti. The hypoeutectic alloys with these eutectics considerably improve the mechanical properties of these alloys [120]. The microstructure of ternary Ti-Fe-Y alloys was found to be similar. These alloys were studied for the laser direct metal deposition process [121]. The addition of Zr in Ti-Fe-Y alloys leads to complex changes in the microstructure. Increasing Zr addition changes the microstructure from hypo eutectic primary TiFe dendrite coexisting with a ternary eutectic of β-Ti + TiFe + Zr_2Fe to a completely eutectic microstructure of β-Ti + TiFe + Zr_2Fe.

Further increase in Zr leads to a hyper eutectic microstructure where eutectic (β-Ti + TiFe + Zr_2Fe) coexist with β-Ti dendrite. The sequence of microstructural changes leads to a gradual decrease in the hardness and Young's modulus [121]. The quaternary eutectic alloys show better mechanical properties, excellent corrosion resistance, and lower Young's modulus than Ti-Fe eutectic alloy and exhibit excellent biocompatibility, including negligible cytotoxicity and early adhesion and proliferation of cells that make them attractive for biological application of line implants. Efforts are being made to adopt this alloy for 3-D printing for near-net processing for medical applications [122]. Development of similar alloys was also attempted by the addition of Cu and C [123]. In recent times, an attempt has been made to make this class of complex high strength eutectic alloys affordable by the addition of Cr and Si [124]. The addition of Nb increases the strength of the Ti-Fe binary eutectic. Fig. 16b shows the variation of yield strength and plasticity with Nb

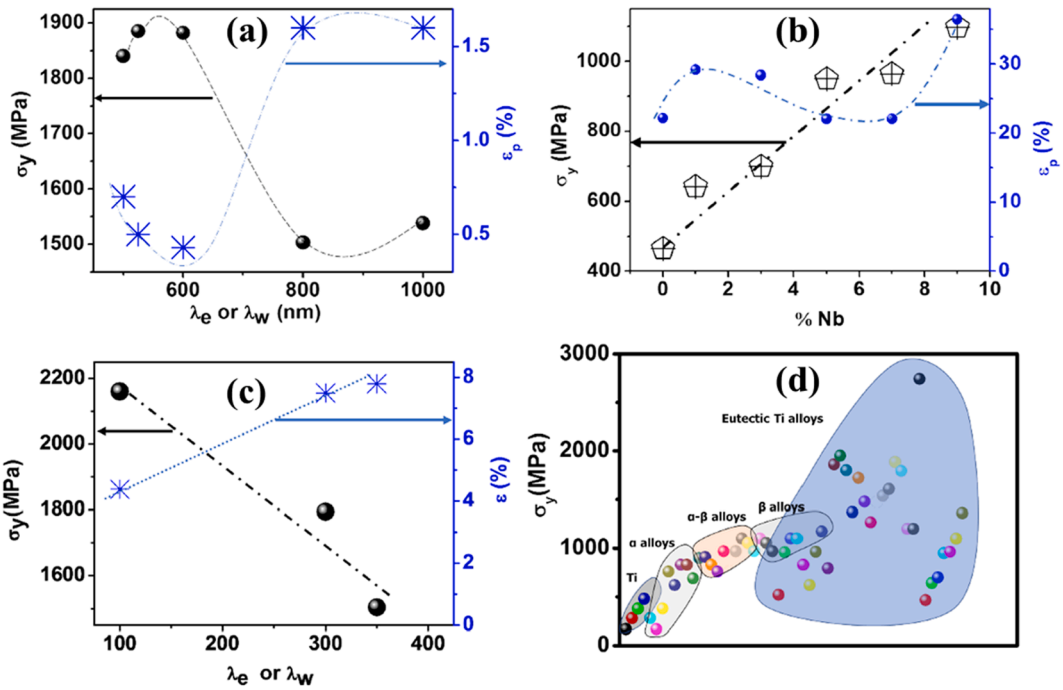

Fig. 16. (a) Variation of yield strength and plastic strain for Ti-Fe eutectic for different lamellar spacing. (b) Variation of yield strength and plastic strain for different concentrations of Nb in Ti-Fe eutectic. (c) Variation of yield strength and plastic strain for Ti-Fe-Sn eutectic for different lamellar spacing. (d) Variation of yield strength for different Ti-based alloys (x-axis is alloys number (a.u.)) [181].

concentration in the ternary eutectic alloy. Further development of the ternary alloys of Ti-Fe class is the synthesis of a series of quaternary and quinary alloys having bimodal microstructure with different microstructural length scale that has resulted in very high strength [95,96]. The alloying additions are Nb and Co combinations, with one report having additional quinary addition of Al [125–127].

4.4. 4.4. Other ternary and quaternary Ti-based eutectics with complex microstructure

Nagarajan *et al.* [128] reported the microstructure evolution and phase stability of rapidly solidified TiNi binary alloys of wide-ranging compositions. At 60 at. % of Ni, the formation of equilibrium eutectic mixture between TiNi and $TiNi_3$ phases is suppressed due to non-equilibrium effects, which leads to the formation of a mixture of glass, TiNi phase, and an ordered metastable phase. The Ti-Ni alloy of eutectic composition is recently used for producing high strength braze joint (700 MPa at 1333 K) [129]. Ternary addition of Nb in Ti-Ni alloys ($Ti_{50-x/2}Ni_{50-x/2}Nb_x$) yields a microstructure dominated by a eutectic mixture of TiNi phase with B2 structure and Nb solid solution [130]. The addition of Cu in the Ti-Ni-Nb alloy (Ti50Ni20Cu20Nb10) yields a sub-micron scale complex microstructure containing ternary eutectics. The intermetallic phases in the structure are the B2 phase (TiNi with Nb replacing Ti sites and Cu replacing Ni sites) and Ti_2Cu with similar replacements by Nb and Cu in the tetragonal Ti_2Cu structure. The alloy yields outstanding mechanical properties with an ultimate compressive and 0.2% yield strength of 1770 MPa and 1000 MPa, respectively, with the plasticity of 11% [131]. A detailed study of phase equilibrium in the Ti-Ni-Sn system indicates the presence of several eutectics that have potential for alloy development. However, no proper evaluation of microstructures and mechanical properties has been carried out [97]. The addition of Si and Al in the Ti-Ni binary eutectic refines the scale of eutectic followed by glass formation [132,133]. Ti-Al-Cr system exhibits an invariant eutectic reaction involving β-Ti solid solution and an $L1_2$ ordered phase $Al_3Ti_{1-x}Cr_x$ having Cu_3Au ordered structure. Depending on the composition, the eutectic coexists with intermetallic compound TiAlCr (C14 structure) and $AlCr_2$(C11b structure). The latter phases often precipitate in the β matrix, strengthening it. The ultimate strength of the hypoeutectic alloys reaches values exceeding 2000 MPa under compression with yield strength close to 600 MPa. The ultimate strength is lower at eutectic composition (~1400 MPa) with a modest drop in yield strength (~550 MPa) [134,135]. The Ti-based alloys of the

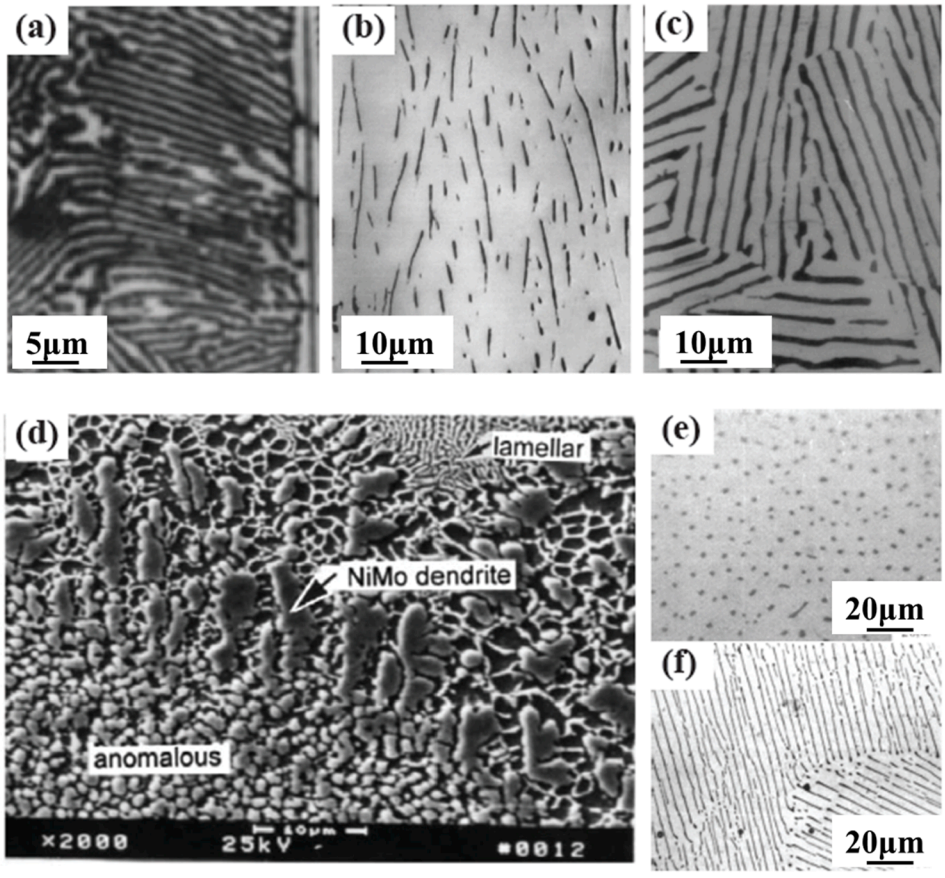

Fig. 17. (a) Solidification microstructures of Ni-32.5 at.% Sn at 49 K [146]. (b) Longitudinal polished section of a eutectic Ni-C specimen frozen at 3.3×10^{-4} cm/sec. (at magnification x235) [145]. (c) Transverse optical micrographs of directionally solidified Ni-Ni_3Si eutectic composite grown at 20.0 mm/h [147]. (d) Microstructure of Ni-Mo alloys at 300 μm tube diameter [149]. (e) and (f) Ni–W microstructure of Transverse section at R = 1.45 cm/h and R = 1 cm/h, respectively [150].

Ti-Al-Nb system also exhibit a eutectic-like structure during solidification containing three intermetallic phases σ-Nb_2Al, γ-TiAl, and η-Al_3Ti.intermetallic phases [136]. Although the microstructure variation in near eutectic alloys is of interest, no study on these alloys mechanical properties is available. A lamellar structure was also reported in a Ti-47Al-2Nb-2Cr-0.2Er alloy with an interlamellar spacing-dependent increase in hardness [137]. The ternary diagram of Ti-Nb-B is of interest because of the presence of a series of borides that can impart potentially useful properties. The alloys containing 7.5 at % B and 17 at.% Nb form eutectic that can be of interest [138]. Replacing Nb with Ge also yields a three-phase eutectic ($Ti_{0.91}Ge_{0.09}$) + Ti_6Ge_2B + (Ti_5Ge_3) in Ti-Ge-B system [139]. In Ti-Si-B ternary system, in addition to binary Ti_{SS}-Ti_3Si eutectic, a three-phase eutectic Tiss + Ti_6Si_2B + Ti_5Si_3 (eutectic) is present [140]. However, mechanical behavior of these eutectic alloys need further probing. The microstructure and phase relations of Ti-Si eutectic alloys have been explored in a limited way with the ternary addition of Zr, Ti and Ga [141]. Recently detailed study of the microstructure and phase equilibrium including the invariant eutectic reactions of Ti-Si-Sn system has been reported [142]. The Ti-Zr-Cu-Al eutectic alloys have been investigated for a possible high strength brazing application for Zircalloy [143]. The mechanical property domain of all the available ternary Ti based eutectic alloys with complex and multimodal microstructure is presented in Fig. 16d. These indicate that it is indeed possible to design a very high strength eutectic alloys of Ti for medium temperature applications if adequate efforts are given to overcome the drawbacks of fracture toughness and proper evaluation of their creep properties.

5. Development of Nickel-based eutectic alloys

Nickel base alloys are the primary driver for high strength, high-temperature alloys that drive the aerospace and energy sectors. Superalloys strengthened by ordered $L1_2$ precipitates are the most important class of such materials [144]. However, Ni also forms several eutectic systems with other alloying elements. These can be of interest if adequate strength, ductility, and high-temperature stability can be imparted by controlling the microstructure. Fig. 17 illustrates a set of representative eutectic microstructures of binary eutectic alloys of nickel. Like the Fe-C system, Ni forms a eutectic with carbon consisting of graphite flake in the Ni matrix (Fig. 17b). Double and Hellawell have studied the flake graphite structure in a Ni alloy with 2.1 wt% C and demonstrated that the graphite becomes finer and irregular or of wavy nature at an increased solidification rate [145]. Ni also forms eutectic with 32 at.% Sn. The morphology of α-Ni/β-Ni_3Sn eutectic structure was studied to gain a fundamental understanding of eutectic growth (Fig. 17a) [145]. The levitation melting of this alloy under glass slag indicates that the eutectic morphology changes from regular lamellar eutectic to irregular anomalous eutectic as undercooling increases. The lamellar eutectic forms under the slow cooling condition, and anomalous eutectic is the rapid solidification product [146]. Similarly, a eutectic reaction occurs at a composition of Ni-11.5 wt% Si (Ni-21.4 at.% Si) at 1416 K [147]. Caram *et al.* have reported the microstructure and morphology of Ni-Ni_3Si eutectic alloy through directional solidification of Ni-rich region of Ni-Si phase diagram (Fig. 17c) [148]. The number of eutectic grains increases with the increase in the growth rate. Undercooling and consequent rapid solidification experiments through drop tube were also carried out on Ni-Mo eutectic to explore the microstructural evolution by employing different diameters of the melt droplets (Fig. 17d) [149]. When drop size is large, lamellar eutectic forms while smaller drop sizes, equiaxed grains of Ni form in large amounts [149]. Another potentially significant binary eutectic is Ni–W eutectic, whose microstructure and crystallography was studied by unidirectional solidification at different growth conditions [150]. The microstructure contains W fibers in Ni(W) matrix. As the solidification rate increases, the structure transforms from lamellar to dendritic, with the direction of growth being along ⟨1 1 1⟩, as shown in Fig. 17e-f. At a slow growth rate (1 cm/h), Ni_4W precipitate is also present in the alloy, opening an additional route for strengthening [150].

5.1. Development of Ni-Al-Cr eutectic alloy

Cr acts as a solid solution strengthener in the Ni-Al system and increases the Ductile-Brittle Transition Temperature (DBTT) [151,152] and oxidation resistance of the alloy [153]. The studies on the quasi binary (AlNi-Cr) eutectic indicate the eutectic reaction

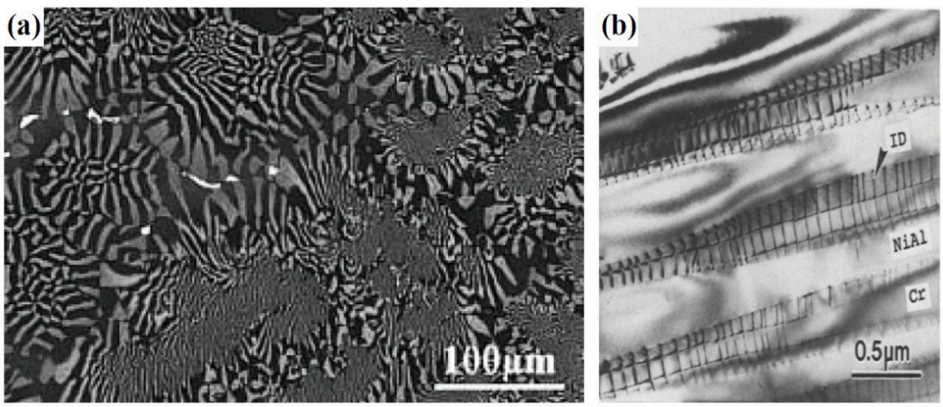

Fig. 18. (a) SEM Micrographs of NiAl-28Cr-6Mo-xTa eutectic alloy where × = 0.5 [157]. (b) TEM micrograph of the interface dislocations (marked 'ID') between the NiAl matrix and Cr-rich metal phase [154].

($L = \alpha + \beta + \gamma$) occurs at 1565 K with the melt composition at 50 at. % Ni and 15.5 at. % Al [40]. The microstructure of NiAl-34Cr eutectic is cellular with a coarse eutectic spacing near the cell boundary in the conventional casting process while fibrous for the directionally solidified alloys [154]. The arrays of discontinuous Cr fibers are aligned parallel to the ⟨1 0 0⟩ growth direction and are embedded in a NiAl matrix. The mismatch along the semi-coherent interface between NiAl and Cr metal is accommodated by a dislocations network, as shown in Fig. 18b. An increase in fracture toughness of these directionally solidified eutectic alloys is due to the crack bridging of second phase. Tiwari *et al.* [151] reported microstructure of the as-cast Ni-43Al-9.7Cr alloy consisting of β-NiAl dendrites and interdendritic NiAl-Cr eutectic with a grain size of 30 μm. Similar study by Walter and Cline [155] on NiAl-34Cr eutectic alloy also confirms the fibrous microstructure, and establish that the Cr inter- rod spacing decreases as $v^{-1/2}$, where v is solidification rate. Solidification rate at 2.54 cm per hour or higher led to cell structure. Same group of authors [156] also reported spheroidization of the fibre when heated at 1673 K for 160 h. The effect of variation of Cr and Al addition on the microstructure of NiAl base alloys with a range of composition 0–5 at.% Cr and 45–52 at.% Al has also been reported [152]. The effect of Ta on the eutectic of NiAl-Cr(Mo) was investigated. Without Ta, the microstructure consists of Cr(Mo) and NiAl eutectic. As the Ta concentration increases, the microstructure deviates from eutectic and the fraction of the NiAl phase increases indicating the effect of Ta in stabilising this phase (Fig. 18a). The yield strength also increases both at room temperature and at 1273 K with the addition of Ta [157]. The alloy with composition NiAl-28Cr-6Mo-0.15Hf exhibits a eutectic microstructure with fibre of Cr(Mo) embedded in NiAl matrix. Addition of Hf into this alloy changes the microstructure. The Ni_2Al_3Hf phase having a hexagonal structure that forms at the interface of NiAl and Cr (Mo). The compression test at 1273 K reveals Hf doped alloy exhibiting higher yield strength than Hf free alloy [158].

Room temperature fracture toughness of the directionally solidified and conventionally cast NiAl-34Cr eutectic alloy are 20.38 and 5.75 MPa.$\sqrt{m}$ (average of the original values), respectively. After heat treating at 1300 K for 500 h, room temperature fracture

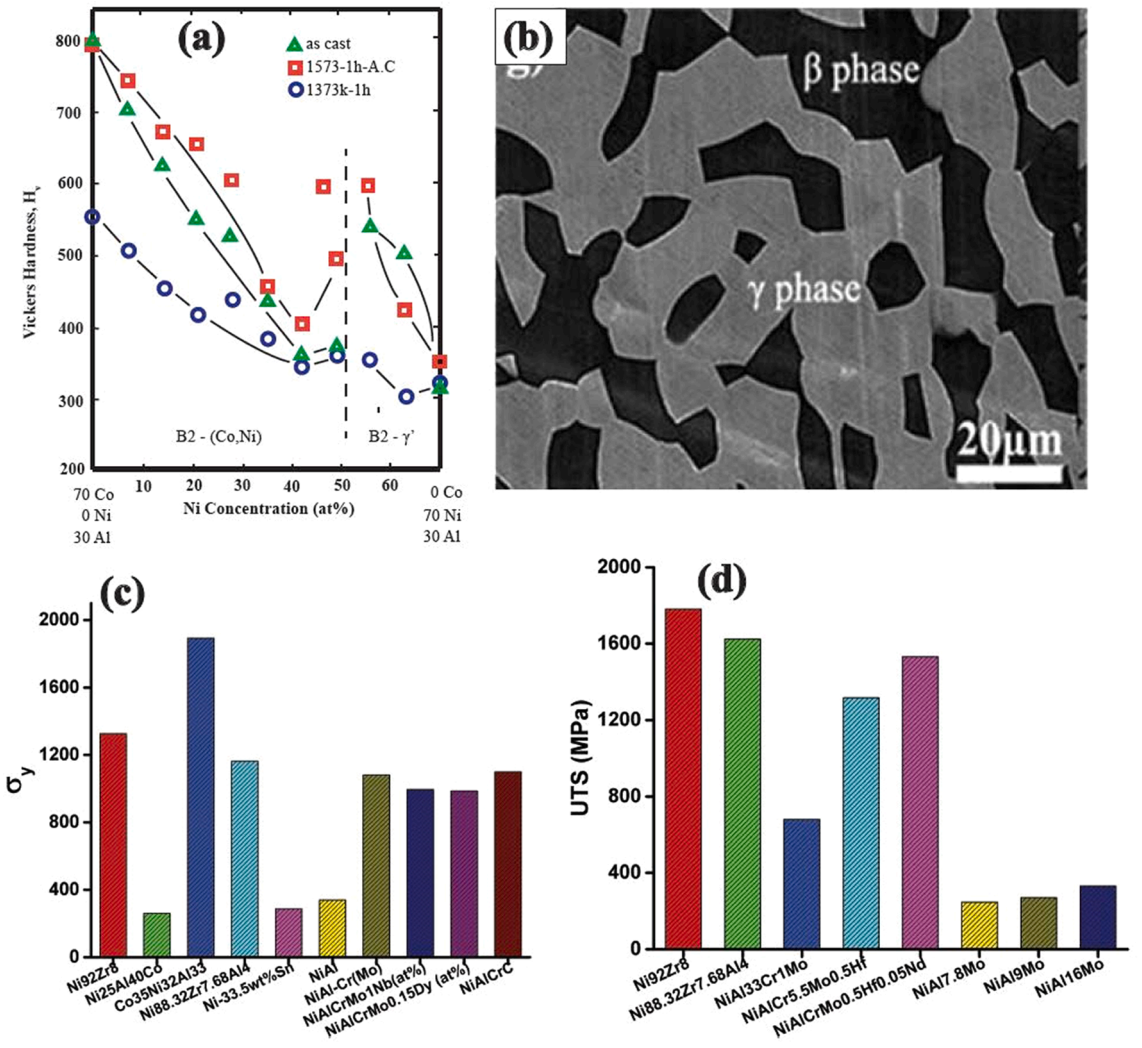

Fig. 19. (a) Micro-Vickers hardness for the Co-Al-Ni alloy [167]. (b) The optical microstructure of alloy 20Ni-60Co-20Al after homogenization and annealing at 1373 K [166]. (c) and (d) Yield stress and ultimate tensile strength comparison of reported Ni-based alloy, respectively [175–183].

toughness of the directionally solidified NiAl-34Cr eutectic alloy is 21.3 MPa.$\sqrt{m}$ [159]. Vickers hardness, yield strength, tensile fracture strength, and elongation of the alloy Ni-20Al-10Cr are 210 DPN, 415 MPa, 700 MPa, and 8.5%, respectively [160]. The yield strength of the alloy Ni-43Al-9.4Cr is reported to be 496 and 446 MPa at 300 and 880 K, respectively, while room temperature fracture toughness is 5.4 MPa.$\sqrt{m}$ [151]. Walter and Cline [155] reported a range of UTS values at high temperatures for the NiAl-34Cr eutectic alloy subjected to different solidification rates that result in variation of Cr rods spacing and shape.

5.2. Development of Ni-Al-Co eutectic alloys

Co addition in Ni alloys improves the resistance to TCP (Topological close-packed phase) formation and lowers the γ' solvus temperature [161,162]. In the Ni-Co-Al system [163], the primary phases present are α-Al, Co_2Al_9, Co_4Al_{13}(HT) (Y1), Co_4Al_{13} (o), $CoAl_3$, Co_2Al_5, D, $NiAl_3$, Ni_2Al_3 and B2. Prominent primary areas are decagonal phase and β-phase denoted by D and B2, respectively. There are nine U-type reactions U_1 to U_9 that can occur during the solidification. The investigation of microstructure of the rapidly solidified Co–(33–40)Ni–(27–29)Al alloys reveals the presence of the coarse primary dendritic of β phase surrounded by $\beta+\gamma$ eutectic structure [164–166]. At lower content of Al, lamellar structure in the eutectic is found to be much thinner, and with increasing cooling rate, a divorced eutectic morphology could be observed. However, at a higher cooling rate, the eutectic reaction could be suppressed. When Al content is increased to 25 at. % and more, martensite structure is observed within the β phase dendrites along with eutectic structure. Liu and Li [165] have reported rapidly solidified $Co_{32}Ni_{40}Al_{28}$ alloy with excellent strength of about 2554 MPa and ductility higher than 17%. The Microhardness of the ternary Ni-Al-Co alloys is shown in Fig. 19a [167]. In alloy composition Ni-20Co-60Al, the eutectic microstructure could be observed, but the eutectic microstructure disappears when annealed at 1373 K resulting in a two-phase ($\beta+\gamma$) structure as shown in Fig. 19b [166]. The alloy with divorced eutectic + martensitic microstructure exhibits a good shape memory recovery of about 75% after thermomechanical processing. The yield stresses and UTS of a series of Ni based alloys are summarised in Fig. 19c.

5.3. Development of NiAl-W/V/Mo eutectic alloys

The phase diagram of NiAI-W exhibits a pseudo-binary eutectic reaction with 1.5% W ($L \rightarrow \beta(NiAl) + \alpha(W)$) at 1937 ± 12 K [168]. Milenkovic *et al.* [169] investigated the pseudo-binary section of NiAl-W in the range 0.7–1.8 at.% W, while Gao *et al.* [170] have investigated the microstructure and microhardness of these eutectic alloys at different growth rates. In the initial growth stage, W forms as the primary phase with dendritic morphology. With increasing growth rate, the dendritic phase disappears due to growing competition between primary W and the eutectic. The eutectics with increasing growth rates exhibit a decreasing trend in fibrous spacing. The presence of W nanoparticles can be observed within the NiAl matrix with a size of 20–50 nm that contributes to the increase in strength of NiAl-W eutectic alloys [170]. A similar eutectic structure was also observed in NiAl-Mo and NiAl-V systems. In the latter case, the eutectic occurs at NiAl-39at.% V with the onset of eutectic reaction at 1639 K [171]. The microstructure and mechanical properties of eutectic alloys of NiAl-Mo with additions of various amounts of Re were studied by Misra *et al.* [172].

The eutectic reaction occurs at ~ 1873 K for a reaction involving the NiAl and Mo phase at a composition of 10 at.% Mo [173]. The element Re has a pronounced effect on the NiAl-Mo eutectic alloys [172]. The orientation relationship between the NiAl and Mo rich phase was cube on cube, and growth direction was typically 15–20° off-$\langle 0\,0\,1\rangle$ NiAl. However, Re containing NiAl-Mo alloy showed dendritic + eutectic microstructures with the inferior alignment of fibers. The compressive strength of NiAl-Mo(Re) was lower than the eutectic NiAl-9Mo alloy due to the poor alignment of fiber. The fracture toughness of NiAl-9Mo was found to be ~ 14.5 MPa.$m^{1/2}$. A decrease in fracture toughness was observed with the addition of Re [172]. The NiAl matrix in the NiAl-Mo system exhibit higher strength that can be attributed to the dispersion of Mo inside the NiAl matrix like that observed for the NiAl-W system. The motion of dislocation inside NiAl gets hindered at the interface between NiAl and Mo due to the lower coherency between the two phases [174].

5.4. Development of Ni-Al-RE (Rare Earth) alloys

The addition of rare earth elements (Ce, Y, Nd, and Dy) into the NiAl based eutectic alloys can influence their microstructure and compressive properties [175]. The element Dy is mainly dispersed at the boundary between eutectic cells. The addition of other RE's (Ce, Nd, and Y) in NiAl-28Cr-5.5Mo-0.5Hf alloy also exhibits a similar effect on the microstructure. The 0.05 wt% Ce doped alloy at room temperature exhibits 14.8% compressive ductility than 9% for RE-free alloys. Compressive strength of 1531 MPa is achieved for the same alloy, which is higher than 1316 MPa reported for the RE-free alloy [175]. Fig. 9c& d presents the yield strength and UTS of different Ni-based eutectic alloys to enable a comprehensive view of mechanical properties these alloys [175–183].

6. Intermetallic based eutectic alloys

The Ni-based superalloys have evolved through the addition of a large number of alloying elements and processing optimization to make them one of the most useful materials for high-temperature applications. The combination of directional solidification (DS), single-crystal processes, and powder metallurgy-based processing techniques leads to further improvement in properties. However, newer developments in structural ceramics like SiC and Si_3N_4 are challenging the supremacy of Ni alloys at higher temperatures. As a new class of high-temperature materials, intermetallics can serve as the bridge between metals (superalloys or refractory metals) and promising structural ceramics. There exist several intermetallics which possess sufficient metal-like behavior but having properties

that cannot be realized in traditional alloys for giving a competitive edge over the newer ceramics. Intermetallic compounds having B2, $L1_2$, and DO_3 crystal structures are most common and useful among 41 high-temperature intermetallics [184,185]. Among these, aluminides of Fe (FeAl and Fe_3Al), Ti (Ti_3Al and TiAl), and Ni (Ni_3Al and NiAl) are most extensively studied, followed by silicides of refractory elements.

There is enormous potential to develop newer materials through eutectic composites of intermetallics with multiple phases with multi-modular distribution, finer and varying length scales. A common intermetallic eutectic is NiAl alloyed with other high-temperature metals such as Cr, Mo, or Nb. It forms NiAl-X (X = Cr, Mo and Nb) in-situ eutectic composites [184,185]. These exhibit a good enhancement in ductility at room temperature. However, the difference in their linear coefficient of thermal expansion (CTE) gives rise to an interface mismatch that leads to poor high-temperature mechanical properties. The eutectic of two intermetallics having similar CTE can overcome this problem. Therefore, several attempts have been made to develop an in-situ grown $Ni_3Al(L1_2)$-$Ni_3V(D0_{22})$ eutectic composites with both phases being intermetallic [186–188]. However, these alloys did not show significant ductility. Significant efforts are undertaken to develop NiAl and Ni_3Al based eutectic alloys [189,190]. These belong to the Ni-rich portions of the Ni-Al-X ternary phase diagram, where X is a group IV element of the periodic table such as Ti, Zr, or Hf. Among these, the Zr doped Ni-Al-Cr-Ta-Mo alloys with intermetallic γ'(Ni_3Al)/β(NiAl) microstructure exhibits improved room temperature ductility [191,192]. The effect of Zr on the properties of these Ni-based intermetallics is complex. Besides the solid solution strengthening of polycrystalline Ni_3Al, Zr increases the room temperature fracture strain and improves corrosion resistance in oxygen-deficient chlorinating atmospheres, and protects Ni_3Al surface against hydrogen permeability [193]. However, increasing Zr content increases oxygen penetration depth along the grain boundaries and forms $\gamma + Ni_5Zr$ eutectic with Ni at 1443 K. It causes embrittlement of Ni_3Al alloys after heat treatments [194]. To date, the maximum Zr content in important commercialized Ni aluminides IC221M (Ni-Al-8.21; Cr-7.61; Zr-2.09; Mo-1.52) is ~ 2 at.% [195]. The as-cast structure contains three phases, ordered Ni_3Al (γ'), Ni solid solution (disorder fcc), and Ni_5Zr intermetallic phase. Lee *et al.* [196] postulated that Ni_5Zr solidified in the interdendritic region to a eutectic type structure with Ni_{ss}, leading to good casting and welding properties. The slow diffusion of Zr leads to improvement in high-temperature strength and creep resistance. The Zr could form a very adherent oxide scale both during cyclic oxidation and isothermal oxidation.

The temperature for the binary eutectic reaction $(L \rightarrow \gamma + Ni_5Zr)$ in the Ni-Zr system, determined by DTA, is 1469 K and increases with Al addition to reach or exceed 1479 K forming a saddle point before decreasing to reach 1460 K or below to undergo a ternary invariant reaction $(L \rightarrow \gamma + \gamma' + Ni_5Zr)$[14]. Other invariant reactions in the ternary system are $L \rightarrow Ni_7Zr_2 + \gamma + Ni_5Zr$, $L + \gamma' \rightarrow Ni_7Zr_2 + \gamma$, and $L \rightarrow Ni_7Zr_2 + \gamma + \beta$.

An extensive research program at the Indian Institute of science recently explored the composites of intermetallic eutectics in the Ni-Al-Zr system at the Ni-rich end, which can replace Ni-based superalloys [14,197–200]. Tiwary *et al.* [200] studied the binary eutectic (E1) $Ni_3Al + Ni_5Zr$, (E2) $Ni_3Al + Ni7Zr_2$, (E3)$NiAl + Ni_7Zr_2$, and the ternary eutectic (TE) $NiAl + Ni_3Al + Ni_7Zr_2$. The eutectic colonies in alloy E3 show a central lamellar structure that degenerates to a more irregular appearance at the boundaries. In contrast, the eutectic in alloy E2 is characterized by an extremely fine fibrous structure. The eutectic in alloy E1 region exhibits a central region of fine regular lamellar structure surrounded by a coarser irregular lamellar morphology. Combinations of two binary eutectics $Ni_3Al + Ni_7Zr_2$ and $NiAl + Ni_7Zr_2$, were also reported. These alloys complex microstructure results in a multi-fold improvement in mechanical properties that needs further study (Fig. 20). The eutectic alloys of the Ni-Al-Zr system exhibit excellent mechanical and oxidation properties. Tiwary *et al.* [200] have reported eutectic structures composed of Ni_3Al, NiAl, Ni_5Zr, and Ni_7Zr_2 intermetallics exhibiting ultra-high strength of about 2.5 GPa, tensile plasticity of about 3–4%, and exceptional oxidation resistance at 1373 K.

Chen *et al.* [201] studied phase relations in more than 60 ternary alloy compositions. Based on the microstructure, isothermal

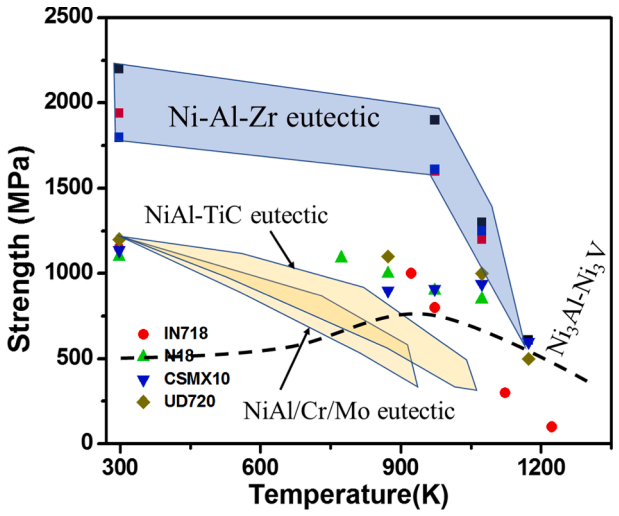

Fig. 20. Variation of yield strength vs. temperature of different Ni-based alloys [14].

sections at 1123 K and 1323 K were reported. A modified liquidus by Ghosh *et al.* [13] (Fig. 21a) shows the ternary eutectics of Ni + Ni_3Al + Ni_5Zr and Ni_3Al + NiAl + Ni_7Zr_2 phases in addition to two possible pseudo-binary reactions (Ni, Al) + Ni_5Zr at 1469 K and Ni_3Al + Ni_7Zr_2 at 1466 K. Tiwary et al. used a different approach to predict the ternary phase diagram and made detailed experimental validation. One of the highlights of the Ni-Al-Zr system is the development of multiphase microstructure during solidification [200]. The Ni_3Al-Ni_5Zr eutectic alloy shows two different morphology for the same eutectic (Fig. 21b). The lamellar colony of eutectic, distributed randomly in the microstructure, is surrounded by a slightly degenerated lamellar eutectic (Fig. 21e-f).

The first type of growth occurred at a higher temperature. The growth is restricted and could not follow the rapid temperature change during suction casting, leading to the rest of the melt's undercooling. The latter undergoes further eutectic transformation yielding the degenerated eutectic. The process is similar to the modification of the eutectic alloys often observed in binary eutectics. The fraction of the two eutectics, Ni_3Al-Ni_7Zr_2 eutectic and NiAl-Ni_7Zr_2 eutectic (Fig. 21c-d), can be controlled by varying compositions. The NiAl-Ni_7Zr_2 eutectic has a fibrous morphology and is more refined than other eutectics. This eutectic is present in the intercellular regions (Fig. 21c-d). Further, the Ni_7Zr_2 rods tend to branch as it grows (Fig. 22).

The Ni_3Al-Ni_7Zr_2 eutectic exhibits a coupled growth. Under the condition of suction casting, the eutectics exhibit a unique cellular/dendritic growth morphology [14]. A low magnification optical micrograph reveals a central stem with distinctly different contrast than the rest of the dendrite. At higher magnification, the central stem gets resolved to reveal a well develop lamellar eutectic microstructure containing plates of the Ni_7Zr_2 in the Ni_3Al matrix. This dendritic growth of the lamellar eutectic resembles the classical dendritic growth of single-phase alloys at a high growth rate. There is a transition of the tip radius of the growing dendrite with growth velocity. The thick and fat dendrite, with increasing growth velocity, undergoes a transition to a plate-like dendritic growth similar to the single-phase growth at a higher growth rate. Careful observation reveals tip splitting of the eutectic dendrites leading to a fractal dendritic morphology similar to that observed in single-phase dendrites. It is well established that anisotropy in surface energy at the dendritic tip stabilizes the tip and leads to a stable dendritic morphology. In case the anisotropy approaches zero, the tip becomes unstable and spontaneously split leading to a fractal dendrite. The cellular/dendritic growth of the eutectic is well known and generally

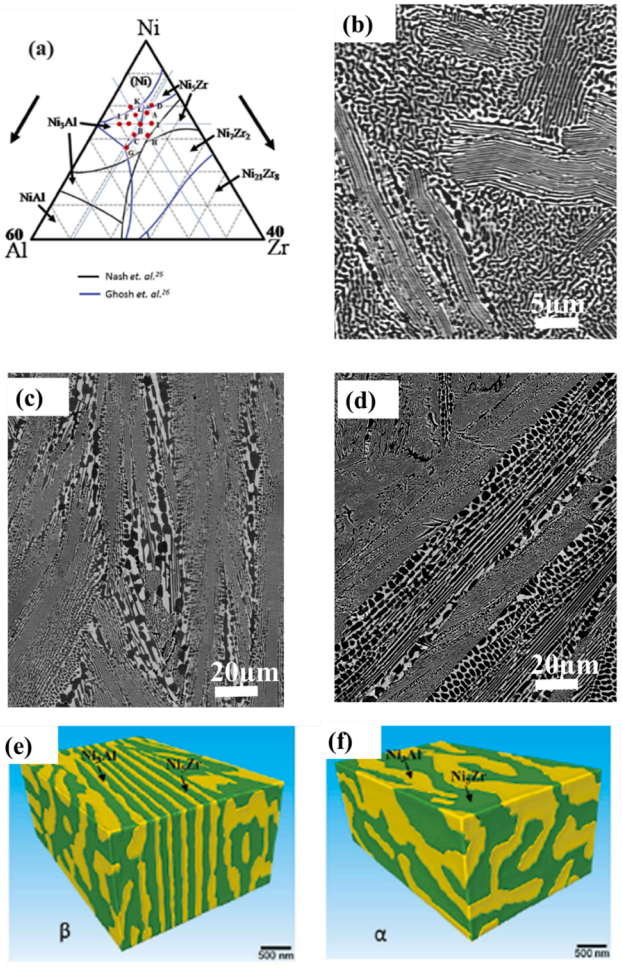

Fig. 21. (a) Ternary liquidus projection of Ni-Al-Zr ternary system. (b) Ni_3Al-Ni_5Zr, (c), and (d) Ni_3Al-Ni_7Zr_2 and NiAl-Ni_7Zr_2 eutectic, respectively. (e) and (f) 3D images of Ni_3Al-Ni_5Zr [14,200].

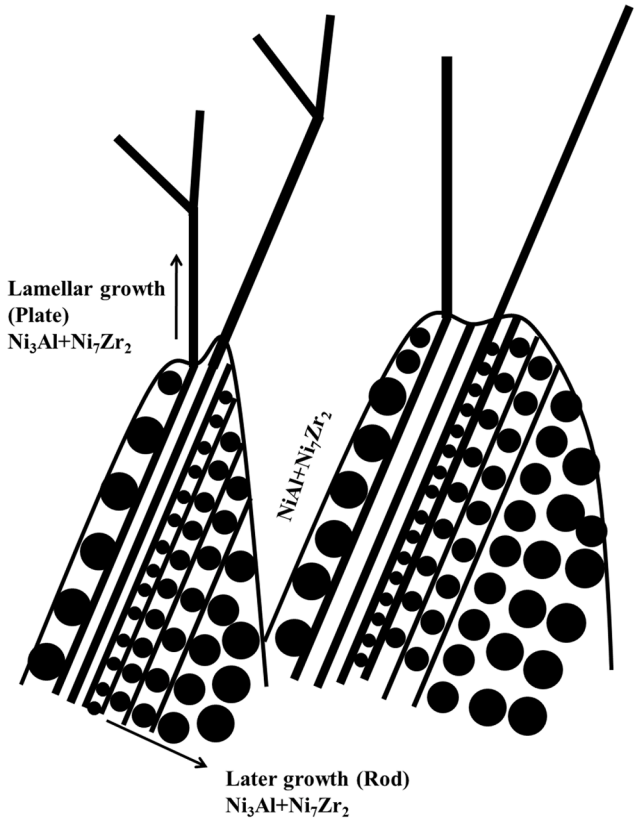

Fig. 22. Growth of Ni_3Al-Ni_7Zr_2 and NiAl-Ni_7Zr_2 eutectic.

attributed to the rejection of impurity at the growing liquid-solid interface. The mechanism of such growth has not been rigorously studied. However, the impurity segregation at the interface leads to a multi-component melt that allows the growth to occur over a range of temperatures. The supersaturation ahead of the plane front can lead to a breakdown of the front leading to cellular dendritic growth. A similar argument can be used to explain the lamellar eutectic's dendritic growth in the ternary alloys.

A more startling observation is the lamellar plate to rod transition behind the growing tip as the cell thickens with rods growing normal to the plates. The rods get coarser as it approaches the cell edge. The evidence of a spiral growth of these rods has been reported, and simulation of such growth in three dimensions is available [202]. The rod eutectic that forms during thickening also gets coarser reflecting the decrease in the growth rate due to either the recalescence of the melt or a concentration gradient developing in the melt approaching the concentration of the second eutectic. More careful experiments and theoretical modeling need to be undertaken in the future to understand this complex morphology.

Although the mechanical properties of Ni_5Zr and Ni_7Zr_2 are not available, the picoindentation studies show that the hardness and modulus of these phases are higher than that of Ni_3Al and NiAl and that Ni_7Zr_2 is the strongest of the four intermetallics that constitute the eutectics studied in this work [14]. However, the eutectic Ni_3Al + Ni_5Zr has the highest yield strength. The yield strength of eutectic composites drops significantly at 973 K due to the decrease in yield strength of the Ni_3Al and NiAl phases at this temperature [200]. However, the temperature and grain size dependence of the strength of Ni_5Zr and Ni_7Zr_2 is not available. Fracture initiation and failure in the eutectic alloys appear to be determined by extensive plasticity in the Ni_3Al, and NiAl phases with void nucleation at Ni_3Al/Ni_5Zr, Ni_3Al/Ni_7Zr_2 or $NiAl/Ni_7Zr_2$ interfaces. No macroscopic brittle behavior could be observed in the fine eutectic structures. The room temperature tensile ductility of 3–4% is quite attractive for the high yield strength achieved in these structures.

7. BCC metal silicides

The refractory metal silicide intermetallics have drawn considerable attention for structural applications. However, the research is primarily geared towards multiphase materials. The second phase is either another silicide or a metallic material either in thermodynamic equilibrium with the silicide under consideration (e.g., Nb-Nb_5Si_3 or Cr-Cr_3Si) or artificially introduced with the hope of capitalizing on possible lack of reactivity or sluggish kinetics. Currently, the evaluation of refractory silicides for very high-temperature applications is aggressively pursued [203,204]. Still, there is no indication that any relevant silicide of Fe, Cr, Mo, Ti, and Nb will ever be used in the monolithic form for such applications in the near future as they lack the required damage tolerance. The composites of the silicides (where the reinforcing phase imparts the damage tolerance) are being examined for high-temperature

application, particularly in the non-rotating components [203–206].

Nb-silicides are an important class of Nb alloys developed in the last two decades. The Si addition reduces the density and improves oxidation and wear resistance. The eutectic alloys consisting of Nb and silicide intermetallic results in a good strength and low density. The interlamellar spacing of the eutectic can be tuned with varying the Si content and cooling rate. However, these alloys have low room temperature ductility and fracture toughness. In a series of work, Kashyap et al. explored ternary addition (Ga, Al, In, Mg, and Ni) in the eutectic composition that can reduce interlamellar spacing and modify the morphologies [207–211]. The submicron spacing results in an improvement in ductility and fracture toughness (Fig. 23). The Al addition results in fine precipitates, which improves room temperature and high-temperature strength. The addition of In modifies the phases present in the eutectic microstructure and results in high strength, good ductility, and oxidation resistance [211]. The other alloying additions such as Mg and Ni refines eutectic and form non-equilibrium phases, resulting in improved mechanical properties and oxidation. The refinement in eutectic also results in an improvement in fracture toughness.

8. Eutectic concentrated multicomponent high entropy alloys

Recently, multicomponent high entropy alloys (HEAs) have attracted considerable interest in alloy development because of their unique microstructure and attractive properties [212]. The HEA concept for new alloy development was started by B. Cantor [213] and J.W. Yeh [214] in 2004. The initial research on HEAs was mainly focused on finding single-phase multi-principle multi-component elemental solid solutions. The strategy was based on “mixing multi-principal elements” in high concentration to synthesize a new class of solid solution alloys. The matrix can be termed a whole solute matrix as no host lattice for the solute can be identified. The sustained efforts by Professor Cantor led to the discovery of the equiatomic CoCrFeMnNi FCC solid solution phase [215]. Following this, other types of HEAs consisting of multiple phases were developed [216,217]. One of these types is eutectic high entropy alloys (EHEAs), forming a subset of HEAs as they exhibit biphasic or triphasic microstructure with predominantly lamellar and a few rod eutectics [218]. Four different types of eutectic microstructures have been discovered till date in the EHEAs; (a) solid solution/solid solution (FCC/BCC, BCC/HCP), (b) solid solution/intermetallic compound (IMC); (c) IMC/IMC and (d) eutectic phases having nanoscaled embedded precipitates. The solid solutions can be either disordered or ordered compounds (B2, $L1_2$, etc.) that contain multiple elements. Predominantly, five different IMCs are reported having crystal structures of $L1_2$, B2, Laves (hexagonal, C14 and C15), μ and σ phases. EHEAs, due to the presence of multiple elements are expected to show promising mechanical properties due to extreme refinement of the lamellar spacing and large solid solution hardening and lattice distortion. A sluggish diffusion in HEAs may

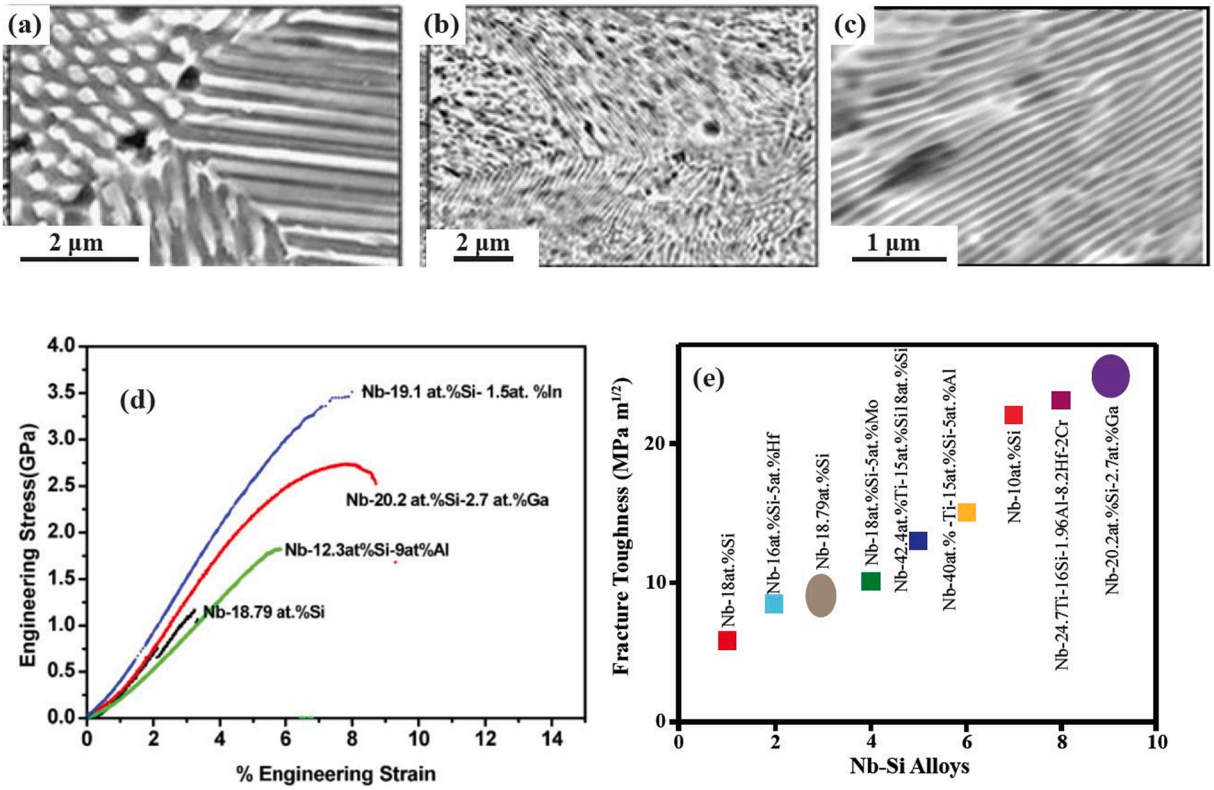

Fig. 23. (a) Nb-Si, (b) Nb-Si-Ga and (c) Nb-Si-Al eutectic alloys. (d) Engineering stress vs. strain plot of Nb-Si based alloys. (e) Fracture toughness of different Nb-Si based alloys [207–209,211].

lead to high creep resistance, microstructural and thermal stability at high temperature and can be used as potential candidates for structural applications [219]. Beside fine eutectic structure, possibility of the formation of multiple primary dendritic phases with varying size and the intermetallic phases can lead to ultrastrong materials [220]. The major drawback that needs to overcome is the issue of ductility for structural application. During secondary processing, plastic deformation led to the reduction of chemical ordering in $AlCoCrFeNi_{2.1}$ EHEA, which may help overcome the ductility issue [221]. Post-processing of EHEAs like $AlCoCrFNi_{2.1}$ also can lead to nanoscaled precipitation of ordered phases in the supersaturated FCC/BCC solid solution lamellae, causing improvement of strength without much compromise on ductility. Therefore, vigorous research activity is ongoing to circumvent the strength-ductility trade-off. EHEAs can be designed by adopting a strategy of developing heterogeneous microstructure consisting of soft solid solution phases and hard intermetallics to achieve a good combination of strength and ductility. In the following, we shall highlight salient features of EHEAs and the way forward.

Samal *et al.* [222] reported high strength in NiTiCuCoTa quinary alloy (strength ∽1988 MPa and plasticity ∽13.5%) developed by reducing interlamellar spacing (λ) from 125 to 75 nm. It could be achieved due to sluggish diffusion that leads to nanoscale microstructure during eutectic solidification and solid solution strengthening. Different alloy design strategies utilizing mixing enthalpy [223], a simple mixing method [224], thermodynamic modeling using CALPHAD method with the aid of available HEA databases [225], high throughput experimentation as well as machine learning [226] have been reported in the literature. The development of EHEA's with a solid solution of five elements and hard intermetallics is well documented in the literature [227–230]. Recently, Rahul *et al.* reported the design and development of seven components ($Co_{10}Cr_{15}Fe_{35\text{-}X}$ $Mn_5NbxNi_{25}V_{10}$ (x = 0, 8.66, 9.5, 9.7, 9.73, 9.8 at%)) EHEAs between FCC solid solution phase and Nb-rich Laves phase with HCP structure using suction casting route, guided by CALPHAD predictions[225]. Due to the reduced length scale of microstructural features and the large volume fraction of eutectic, good mechanical properties were reported. Similarly, Jain *et al.* [231] also reported eight components $Fe_{32.5\text{-}x}Co_{10}Ni_{25}Cr_{15}Mn_5V_{10}Al_{2.5}Nbx$ (x = 5, 7.5, 10, and 12.5 at%) EHEAs between FCC solid solution phase and the Co_2Nb-type Laves phase by an integrated approach using thermodynamic simulation and non-equilibrium solidification processing technique. An EHEA has been developed by destabilizing the FCC single phase with the addition of Nb and consequent formation of eutectics consisting of CoCrFeNiV-rich solid solution phase (FCC (α)) and Co_2Nb-type Laves phase (Fig. 24a). Wani *et al.* [232] investigated the microstructure and mechanical properties of heavily cold-rolled and annealed $AlCoCrFeNi_{2.1}$ EHEA and observed that the annealed material shows a superior combination of the ultimate tensile strength (∼1.2 GPa) and ductility (∼12%).

Reports are available of producing multiphase eutectic-like microstructure using processes other than the solidification route. Recently, Han *et al.* [218] reported the development of equiaxed $Co_{25.1}Cr_{18.8}Fe_{23.3}Ni_{22.6}Ta_{8.5}Al_{1.7}$ (at%) EHEA consisting of FCC solid solution phase with nanosized $L1_2$ ordered precipitates and C14 Laves phase by powder metallurgy route phase. These microstructures are shown to be stable for 100 h at a temperature of 1273 K. They have well-balanced mechanical properties such as yield strength (∼800 MPa) and tensile ductility (∼16%) at a temperature up to 1073 K. Recently, the deformation processing map of $AlCoCrFeNi_{2.1}$ EHEA [233], consisting of 100% of eutectics (CoCrFe-rich (fcc) and NiAl-rich phases), has been investigated to identify the regimes of workability. The optimum thermo-mechanical window is 1073–1150 K and strain rate 10^{-3}–$10^{-2.2}$ s^{-1} as well as in the range 1338–1373 K and 10^{-3}–$10^{-1.2}$ s^{-1} (Fig. 24b). Similarly, the hot deformation behavior and processing map of Co-Cu-Fe-Ni-Ti EHEA, consisting of bcc (β) and fcc (α_2) solid solution dendritic phases and eutectics (fcc (α_1) plus Ti_2(Ni, Co)-type Laves phase) have been reported [234]. Some interesting current developments include the design and development of CoCrFeNiZr bimodal eutectics high entropy alloy consisting of globular eutectics (i.e. L ⟶ FCC (α) + Ni_2Zr) and lamellar eutectics (i.e. L ⟶ FCC (α) + Ni_7Zr_2) (Fig. 24c) [235].

Fig. 25 shows the yield strength vs. ductility plot of the available alloys of EHEAs. The plot indicates that it is possible to develop very high-strength structural materials using EHEA. The highest strength can be obtained for the BCC + IMC EHEAS. However, considering the issue of plastic strain, FCC + IMC EHEAs are more attractive. The ongoing activities by various research groups worldwide indicate that several fundamental issues in this emerging field of EHEAs need to be addressed to make EHEAs the potential candidates for high-temperature structural applications. However, this is truly an emerging field for developing high-strength eutectic alloys for structural applications.

9. Summary and way forward

In the present review, we tried to highlight that eutectic alloys represent new opportunities for developing high-strength structural materials. The initial investigation on the evolution of coupled microstructure during the eutectic reaction in binary alloys led to few important engineering materials which are widely used. However inherent brittleness of other eutectic alloys stalled further work. The recent interests in ternary and higher-order eutectic alloys revealed the possibility of evolution of complex microstructure aided by new solidification techniques, including rapid solidification techniques and laser aided processing that allow control on the length scale of these microstructures to a nanometric level. The emergence of nanoeutectics and multi-modular structures with varying length scales profoundly influences alloy development with eutectic microstructure. The decreasing length scale strengthens the eutectic alloy. Still, the coupling of multi-modular microstructure (including the coexisting primary phases) and length scale allow accommodation of micro-strains and introduce localized shear banding that improves plasticity and fracture toughness. Thus, as reviewed in this article, the complex eutectics represent an opportunity for developing a new class of ultrahigh strength materials. However significant challenges remain to fructify this potential. Scaling these materials without compromising the microstructures, as well as properties, represents a significant challenge. Designing microstructure with reduced length scale through additive manufacturing, alloying, and diffusion control are some of the possible ways to address this challenge. The long-term stability at elevated operating temperatures and their environmental compatibilities will remain an important issue for any complex microstructure with varying

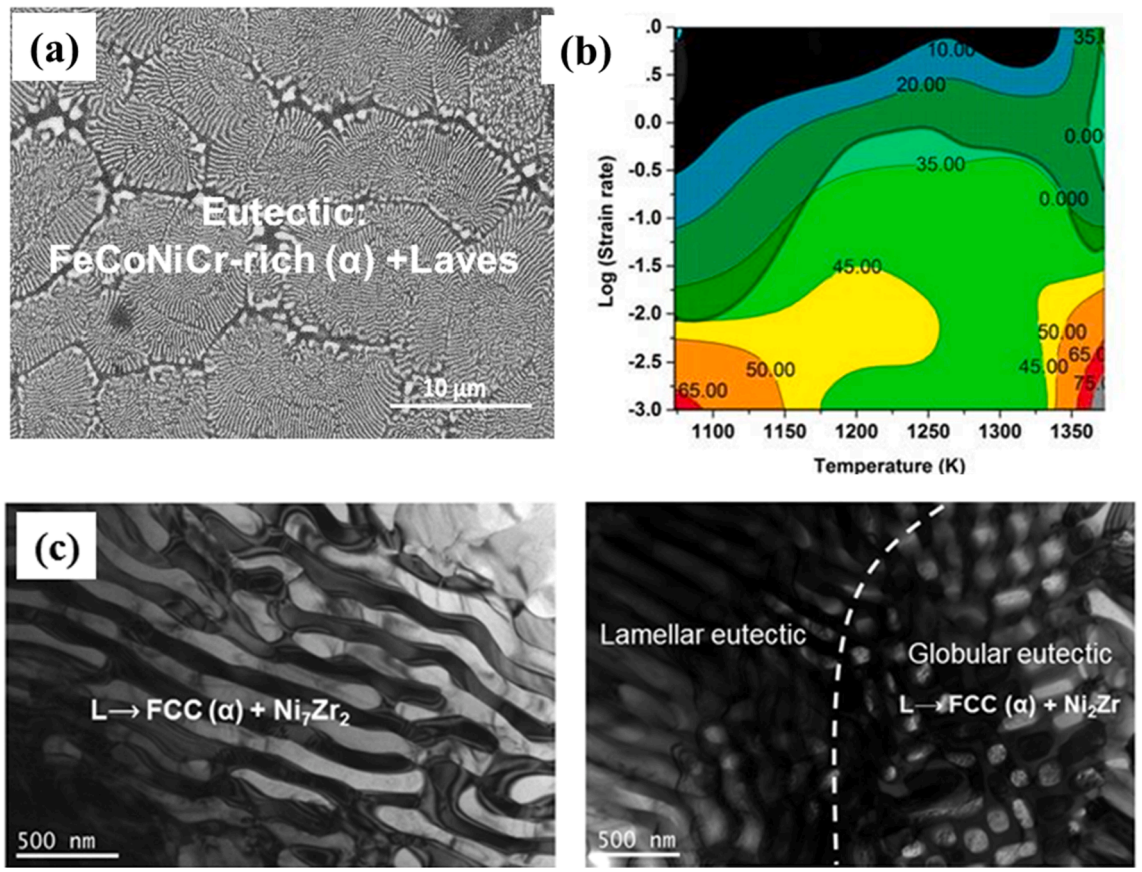

Fig. 24. (a) BSE-SEM micrograph of $FeCoNiCrMnVAlNb_x$ HEA with $\times$ = 7.5 at. %. (b) Deformation processing maps of $AlCoCrFeNi_{2.1}$ EHEA [233]. (c) TEM micrographs of the multicomponent $(CoCrFeNi)_{90}Zr_{10}$ QHEA [235].

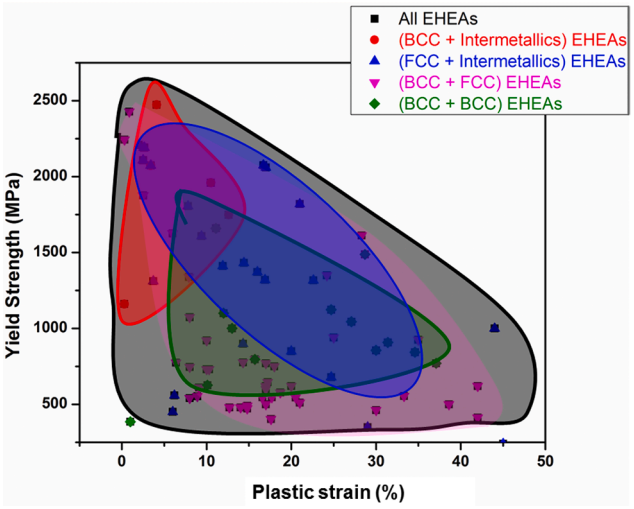

Fig. 25. Yield strength vs. plastic strain of different EHEAs.

length scale and compositions. The research efforts on the related coarsening studies and creep behavior are very few and need to be undertaken in the future. Many of the ultrahigh-strength eutectic materials will have limited ductility. The use of such materials efficiently requires a shift in design philosophy as it is considered for high-strength structural ceramics. However, length scale controlled complex multi-modular eutectics demands attention as a new class of futuristic high strength material.

Declaration of Competing Interest

The authors declare that they have no known competing financial interests or personal relationships that could have appeared to influence the work reported in this paper.

Acknowledgments

One of the authors (KC) acknowledges the Science and Engineering Research Board of the Department of Science and Technology, Government of India, for support through the distinguished fellowship program. CST acknowledges Ramanujan Fellowship. CST acknowledges Science and Engineering Research Board of the Department of Science and Technology, Government of India, for support through the core research grant.

References

[1] Chadwick GA. Eutectic alloy solidification. Prog Mater Sci 1963;12:99–182. https://doi.org/10.1016/0079-6425(63)90037-9.
[2] Cantor B, May GJ, Chadwick GA. The tensile fracture behaviour of the aligned Al-Al3Ni and Al-CuAl2 eutectics at various temperatures. J Mater Sci 1973;8:830–8. https://doi.org/10.1007/BF02397911.
[3] Cantor B, Chadwick GA. The tensile deformation of unidirectionally solidified Al-Al3Ni and Al-Al2Cu eutectics. J Mater Sci 1975;10:578–88. https://doi.org/10.1007/BF00566564.
[4] Cantor B, Chadwick GA. The growth crystallography of unidirectionally solidified Al-Al3Ni and Al-Al2Cu eutectics. J Cryst Growth 1974;23:12–20. https://doi.org/10.1016/0022-0248(74)90035-9.
[5] Chadwick GA. Structure and properties of eutectic alloys. Metal Sci 1975;9:300–4. https://doi.org/10.1179/030634575790444441.
[6] Hunt JD, Jackson KA. Trans TMS-AIME 1966;236:843–52.
[7] Jackson KA, Hunt JD. Trans TMS-AIME 1966;236:1129–42.
[8] Kurz W, Fisher DJ. Fundamentals of Solidification | Book | Scientific.Net; n.d. https://www.scientific.net/book/fundamentals-of-solidification/978-3-0357-3239-9 (accessed August 17, 2020).
[9] Trivedi R, Magnin P, Kurz W. Theory of eutectic growth under rapid solidification conditions. Acta Metall 1987;35:971–80. https://doi.org/10.1016/0001-6160(87)90176-3.
[10] Kurz W, Trivedi R. Eutectic growth under rapid solidification conditions. MTA 1991;22:3051–7. https://doi.org/10.1007/BF02650266.
[11] Plapp M, Karma A. Eutectic colony formation: A phase-field study. Phys Rev E 2002;66:061608. https://doi.org/10.1103/PhysRevE.66.061608.
[12] Ghosh S, Choudhury A, Plapp M, Bottin-Rousseau S, Faivre G, Akamatsu S. Interphase anisotropy effects on lamellar eutectics: A numerical study. Phys Rev E 2015;91:022407. https://doi.org/10.1103/PhysRevE.91.022407.
[13] Karma A, Plapp M. New insights into the morphological stability of eutectic and peritectic coupled growth. JOM 2004;56:28–32. https://doi.org/10.1007/s11837-004-0069-7.
[14] Tiwary CS. Microstructural, Mechanical and Oxidation behavior of Ni-Al-Zr Teranry alloys. IISc, Bangalore; 2014.
[15] Seidman DN, Marquis EA, Dunand DC. Precipitation strengthening at ambient and elevated temperatures of heat-treatable Al(Sc) alloys. Acta Mater 2002;50:4021–35. https://doi.org/10.1016/S1359-6454(02)00201-X.
[16] Knipling KE, Dunand DC, Seidman DN. Precipitation evolution in Al–Zr and Al–Zr–Ti alloys during aging at 450–600°C. Acta Mater 2008;56:1182–95. https://doi.org/10.1016/j.actamat.2007.11.011.
[17] Knipling KE, Dunand DC, Seidman DN. Criteria for developing castable, creep-resistant aluminum-based alloys – A review. Zeitschrift Für Metallkunde 2006;97:246–65. https://doi.org/10.3139/146.101249.
[18] Knipling KE, Seidman DN, Dunand DC. Ambient- and high-temperature mechanical properties of isochronally aged Al–0.06Sc, Al–0.06Zr and Al–0.06Sc–0.06Zr (at.%) alloys. Acta Mater 2011;59:943–54. https://doi.org/10.1016/j.actamat.2010.10.017.
[19] Mondol S, Alam T, Banerjee R, Kumar S, Chattopadhyay K. Development of a high temperature high strength Al alloy by addition of small amounts of Sc and Mg to 2219 alloy. Mater Sci Eng, A 2017;687:221–31. https://doi.org/10.1016/j.msea.2017.01.037.
[20] Guo JQ, Ohtera K. Microstructures and mechanical properties of rapidly solidified high strength Al–Ni based alloys. Acta Mater 1998;46:3829–38. https://doi.org/10.1016/S1359-6454(98)00065-2.
[21] Tiwary CS, Chakraborty S, Mahapatra DR, Chattopadhyay K. Length-scale dependent mechanical properties of Al-Cu eutectic alloy: Molecular dynamics based model and its experimental verification. J Appl Phys 2014;115:203502. https://doi.org/10.1063/1.4879249.
[22] Pandey P, Kashyap S, Tiwary CS, Chattopadhyay K. Development of high-strength high-temperature cast Al-Ni-Cr alloys through evolution of a novel composite eutectic structure. Metall Mat Trans A 2017;48:5940–50. https://doi.org/10.1007/s11661-017-4369-2.
[23] Milenkovic S, Dalbert V, Marinkovic R, Hassel AW. Selective matrix dissolution in an Al–Si eutectic. Corros Sci 2009;51:1490–5. https://doi.org/10.1016/j.corsci.2008.10.031.
[24] Ardell AJ. Isotropic fiber coarsening in unidirectionally solidified eutectic alloys. MT 1972;3:1395–401. https://doi.org/10.1007/BF02643023.
[25] Smartt HB, Tu LK, Courtney TH. Elevated temperature stability of the Al−Al3Ni eutectic composite. Metall Trans 1971;2:2717–27. https://doi.org/10.1007/BF02814917.
[26] Smartt HB, Courtney TH. The kineticsof coarsening in the AI-AI3Ni system. Metall Trans A n.d. 4.
[27] Tiwary CS, Kashyap S, Chattopadhyay K. Development of alloys with high strength at elevated temperatures by tuning the bimodal microstructure in the Al–Cu–Ni eutectic system. Scr Mater 2014;93:20–3. https://doi.org/10.1016/j.scriptamat.2014.08.020.
[28] Li B, Wang H, Jie J, Wei Z. Effects of yttrium and heat treatment on the microstructure and tensile properties of Al–7.5Si–0.5Mg alloy. Mater Des 2011;32:1617–22. https://doi.org/10.1016/j.matdes.2010.08.040.
[29] Xu C, Xiao W, Hanada S, Yamagata H, Ma C. The effect of scandium addition on microstructure and mechanical properties of Al–Si–Mg alloy: A multi-refinement modifier. Mater Charact 2015;110:160–9. https://doi.org/10.1016/j.matchar.2015.10.030.
[30] Hegde S, Prabhu KN. Modification of eutectic silicon in Al–Si alloys. J Mater Sci 2008;43:3009–27. https://doi.org/10.1007/s10853-008-2505-5.
[31] Flood SC, Hunt JD. Modification of Al-Si eutectic alloys with Na. Metal Science 1981;15:287–94. https://doi.org/10.1179/030634581790426813.
[32] Zuo M, Liu X, Sun Q. Effects of processing parameters on the refinement of primary Si in A390 alloys with a new Al–Si–P master alloy. J Mater Sci 2009;44:1952–8. https://doi.org/10.1007/s10853-009-3287-0.
[33] Hafiz MF, Kobayashi T. Tensile properties influencing variables in eutectic Al-Si casting alloys. Scr Metall Mater 1994;31:701–5. https://doi.org/10.1016/0956-716X(94)90213-5.
[34] Zimmermann M, Carrard M, Kurz W. Rapid solidification of Al-Cu eutectic alloy by laser remelting. Acta Metall 1989;37:3305–13. https://doi.org/10.1016/0001-6160(89)90203-4.
[35] Tiwary CS, Roy Mahapatra D, Chattopadhyay K. Effect of length scale on mechanical properties of Al-Cu eutectic alloy. Appl Phys Lett 2012;101:171901. https://doi.org/10.1063/1.4761944.
[36] Park JM, Mattern N, Kühn U, Eckert J, Kim KB, Kim WT, et al. High-strength bulk Al-based bimodal ultrafine eutectic composite with enhanced plasticity. J Mater Res 2009;24:2605–9. https://doi.org/10.1557/jmr.2009.0297.

[37] De Wilde J, Froyen L, Rex S. Coupled two-phase [α(Al)+θ(Al2Cu)] planar growth and destabilisation along the univariant eutectic reaction in Al–Cu–Ag alloys. Scr Mater 2004;51:533–8. https://doi.org/10.1016/j.scriptamat.2004.05.040.
[38] Hötzer J, Steinmetz P, Dennstedt A, Genau A, Kellner M, Sargin I, et al. Influence of growth velocity variations on the pattern formation during the directional solidification of ternary eutectic Al-Ag-Cu. Acta Mater 2017;136:335–46. https://doi.org/10.1016/j.actamat.2017.07.007.
[39] Genau AL, Ratke L. Crystal orientation and morphology in Al-Ag-Cu ternary eutectic. IOP Conf Ser: Mater Sci Eng 2012;27:012032. https://doi.org/10.1088/1757-899X/27/1/012032.
[40] Huang W, Chang YA. Thermodynamic properties of the Ni–Al–Cr system. Intermetallics 1999;7:863–74. https://doi.org/10.1016/S0966-9795(98)00138-1.
[41] Compton DN, Cornish LA, Witcomb MJ. The effect of microstructure on hardness measurements in the aluminium-rich corner of the Al–Ni–Cr system. J Alloy Compd 2001;317–318:372–8. https://doi.org/10.1016/S0925-8388(00)01441-9.
[42] Liu S, Lee JH, Trivedi R. Dynamic effects in the lamellar–rod eutectic transition. Acta Mater 2011;59:3102–15. https://doi.org/10.1016/j.actamat.2011.01.050.
[43] Rosell-Laclau E, Durand-Charre M, Audier M. Liquid-solid equilibria in the aluminium-rich corner of the Al-Cr-Ni system. J Alloy Compd 1996;233:246–63. https://doi.org/10.1016/0925-8388(95)01988-X.
[44] Grushko B, Kowalski W, Pavlyuchkov D, Przepiórzyński B, Surowiec M. A contribution to the Al–Ni–Cr phase diagram. J Alloy Compd 2008;460:299–304. https://doi.org/10.1016/j.jallcom.2007.06.044.
[45] Grushko B, Kowalski W, Pavlyuchkov D, Mi S, Surowiec M. Al-rich region of the Al–Ni–Cr alloy system below 900°C. J Alloy Compd 2009;485:132–8. https://doi.org/10.1016/j.jallcom.2009.05.093.
[46] Premkumar MK, Lawley A, Koczak MJ. Processing and microstructure of. MTA 1992;23:3219–30. 10.1007/BF03024529.
[47] Bian Z, Dai S, Wu L, Chen Z, Wang M, Chen D, et al. Thermal stability of Al–Fe–Ni alloy at high temperatures. J Mater Res Technol 2019;8:2538–48. https://doi.org/10.1016/j.jmrt.2019.01.028.
[48] Tiwary CS, Kashyap S, Kim DH, Chattopadhyay K. Al based ultra-fine eutectic with high room temperature plasticity and elevated temperature strength. Mater Sci Eng, A 2015;639:359–69. https://doi.org/10.1016/j.msea.2015.05.024.
[49] Průša F, Vojtěch D, Michalcová A, Marek I. Mechanical properties and thermal stability of Al–Fe–Ni alloys prepared by centrifugal atomisation and hot extrusion. Mater Sci Eng, A 2014;603:141–9. https://doi.org/10.1016/j.msea.2014.02.081.
[50] Silva BL, Dessi JG, Gomes LF, Peres MM, Canté MV, Spinelli JE. Assessing microstructures and mechanical resistances of as-atomized and as-extruded samples of Al-1wt%Fe-1wt%Ni alloy. J Alloy Compd 2017;691:952–60. https://doi.org/10.1016/j.jallcom.2016.08.243.
[51] Kim JT, Lee SW, Hong SH, Park HJ, Park J-Y, Lee N, et al. Understanding the relationship between microstructure and mechanical properties of Al–Cu–Si ultrafine eutectic composites. Mater Des 2016;92:1038–45. https://doi.org/10.1016/j.matdes.2015.12.080.
[52] Kim JT, Hong SH, Park JM, Eckert J, Kim KB. Microstructure and mechanical properties of hierarchical multi-phase composites based on Al-Ni-type intermetallic compounds in the Al-Ni-Cu-Si alloy system. J Alloy Compd 2018;749:205–10. https://doi.org/10.1016/j.jallcom.2018.03.313.
[53] Ramakrishnan BP, Lei Q, Misra A, Mazumder J. Effect of laser surface remelting on the microstructure and properties of Al-Al 2 Cu-Si ternary eutectic alloy. Sci Rep 2017;7:13468. https://doi.org/10.1038/s41598-017-13953-5.
[54] Park JM, Kim KB, Kim DH, Mattern N, Li R, Liu G, et al. Multi-phase Al-based ultrafine composite with multi-scale microstructure. Intermetallics 2010;18:1829–33. https://doi.org/10.1016/j.intermet.2010.02.042.
[55] Maity S, Chanda DKr, Ramasamy P, Show BK, Eckert J, Bera S. Evolution of bimodal microstructure and high-temperature wear resistance of Al-Cu-Ni alloys. Metall Mat Trans A 2020; 51: 109–15. 10.1007/s11661-019-05518-0.
[56] Mondol S, Kashyap S, Kumar S, Chattopadhyay K. Improvement of high temperature strength of 2219 alloy by Sc and Zr addition through a novel three-stage heat treatment route. Mater Sci Eng, A 2018;732:157–66. https://doi.org/10.1016/j.msea.2018.07.003.
[57] Kasprzak W, Amirkhiz BS, Niewczas M. Structure and properties of cast Al–Si based alloy with Zr–V–Ti additions and its evaluation of high temperature performance. J Alloy Compd 2014;595:67–79. https://doi.org/10.1016/j.jallcom.2013.11.209.
[58] Lee SW, Kim JT, Hong SH, Park HJ, Park J-Y, Lee NS, et al. Micro-to-nano-scale deformation mechanisms of a bimodal ultrafine eutectic composite. Sci Rep 2014;4:6500. https://doi.org/10.1038/srep06500.
[59] Hu J, Zhang W, Fu D, Teng J, Zhang H. Improvement of the mechanical properties of Al–Mg–Si alloys with nano-scale precipitates after repetitive continuous extrusion forming and T8 tempering. J Mater Res Technol 2019;8:5950–60. https://doi.org/10.1016/j.jmrt.2019.09.070.
[60] Xu C, Xiao W, Zheng R, Hanada S, Yamagata H, Ma C. The synergic effects of Sc and Zr on the microstructure and mechanical properties of Al–Si–Mg alloy. Mater Des 2015;88:485–92. https://doi.org/10.1016/j.matdes.2015.09.045.
[61] Chen Z, Mo Y, Nie Z. Effect of Zn content on the microstructure and properties of super-high strength Al-Zn-Mg-Cu alloys. Metall Mat Trans A 2013;44:3910–20. https://doi.org/10.1007/s11661-013-1731-x.
[62] Pandey P, Makineni SK, Gault B, Chattopadhyay K. On the origin of a remarkable increase in the strength and stability of an Al rich Al-Ni eutectic alloy by Zr addition. Acta Mater 2019;170:205–17. https://doi.org/10.1016/j.actamat.2019.03.025.
[63] Kumar Makineni S, Sugathan S, Meher S, Banerjee R, Bhattacharya S, Kumar S, et al. Enhancing elevated temperature strength of copper containing aluminium alloys by forming L1 2 Al 3 Zr precipitates and nucleating θ″ precipitates on them. Sci Rep 2017;7:11154. https://doi.org/10.1038/s41598-017-11540-2.
[64] Mondol S, Makineni SK, Kumar S, Chattopadhyay K. Enhancement of High Temperature Strength of 2219 Alloys Through Small Additions of Nb and Zr and a Novel Heat Treatment. Metall Mat Trans A 2018;49:3047–57. https://doi.org/10.1007/s11661-018-4614-3.
[65] Yin Z, Pan Q, Zhang Y, Jiang F. Effect of minor Sc and Zr on the microstructure and mechanical properties of Al–Mg based alloys. Mater Sci Eng, A 2000;280:151–5. https://doi.org/10.1016/S0921-5093(99)00682-6.
[66] Niranjani VL, Hari Kumar KC, Subramanya Sarma V. Development of high strength Al–Mg–Si AA6061 alloy through cold rolling and ageing. Mater Sci Eng, A 2009;515:169–74. https://doi.org/10.1016/j.msea.2009.03.077.
[67] Belov NA, Alabin AN, Eskin DG. Improving the properties of cold-rolled Al–6%Ni sheets by alloying and heat treatment. Scr Mater 2004;50:89–94. https://doi.org/10.1016/j.scriptamat.2003.09.033.
[68] Suwanpreecha C, Pandee P, Patakham U, Limmaneevichitr C. New generation of eutectic Al-Ni casting alloys for elevated temperature services. Mater Sci Eng, A 2018;709:46–54. https://doi.org/10.1016/j.msea.2017.10.034.
[69] Suwanpreecha C, Toinin JP, Michi RA, Pandee P, Dunand DC, Limmaneevichitr C. Strengthening mechanisms in AlNiSc alloys containing Al3Ni microfibers and Al3Sc nanoprecipitates. Acta Mater 2019;164:334–46. https://doi.org/10.1016/j.actamat.2018.10.059.
[70] Karlsson B, Lindén G. Plastic deformation of eutectoid steel with different cementite morphologies. Mater Sci Eng 1975;17:153–64. https://doi.org/10.1016/0025-5416(75)90039-7.
[71] Dollar M, Bernstein IM, Thompson AW. Influence of deformation substructure on flow and fracture of fully pearlitic steel. Acta Metall 1988;36:311–20. https://doi.org/10.1016/0001-6160(88)90008-9.
[72] Meng F, Qiu J, Baker I. Effect of Al content on the microstructure and mechanical behavior of two-phase FeNiMnAl alloys. J Mater Sci 2014;49:1973–83. https://doi.org/10.1007/s10853-013-7884-6.
[73] Miller CM, Anderson IE, Smith JF. A viable tin-lead solder substitute: Sn-Ag-Cu. JEM 1994;23:595–601. https://doi.org/10.1007/BF02653344.
[74] Lee LM, Mohamad AA. Interfacial reaction of Sn-Ag-Cu lead-free solder alloy on Cu: a review. Adv Mater Sci Eng 2013;2013:e123697. https://doi.org/10.1155/2013/123697.
[75] Wu CML, Huang ML. Creep behavior of eutectic Sn-Cu lead-free solder alloy. 828–828 J Elec Mater 2002;31. https://doi.org/10.1007/s11664-002-0246-9.
[76] Sun L, Zhang L. Properties and microstructures of Sn-Ag-Cu-X lead-free solder joints in electronic packaging. Adv Mater Sci Eng 2015;2015:e639028. https://doi.org/10.1155/2015/639028.
[77] Moon K-W, Boettinger WJ. Accurately determining eutectic compositions: The Sn-Ag-Cu ternary eutectic. JOM 2004;56:22–7. https://doi.org/10.1007/s11837-004-0068-8.

[78] Lewis D, Allen S, Notis M, Scotch A. Determination of the eutectic structure in the Ag-Cu-Sn system. J Elec Mater 2002;31:161–7. https://doi.org/10.1007/s11664-002-0163-y.
[79] Wang D, Li Y, Sun BB, Sui ML, Lu K, Ma E. Bulk metallic glass formation in the binary Cu–Zr system. Appl Phys Lett 2004;84:4029–31. https://doi.org/10.1063/1.1751219.
[80] Perry AJ. The properties of directionally-solidified eutectic and hypo-eutectic copper-zirconium alloys. J Mater Sci 1973;8:443–50. https://doi.org/10.1007/BF00550167.
[81] Perry AJ. Directionally solidified copper-CuZrSi pseudo-binary eutectic alloys. Mater Sci Eng 1973;11:203–9. https://doi.org/10.1016/0025-5416(73)90079-7.
[82] Saitoh M, Kajihara M, Tomioka Y, Miyake J. Microstructure formed by eutectic reaction in a binary Cu–12.3Zr alloy. Mater Sci Eng, A 2001;318:87–93. https://doi.org/10.1016/S0921-5093(01)01340-5.
[83] Han K, Vasquez AA, Xin Y, Kalu PN. Microstructure and tensile properties of nanostructured Cu-25wt%Ag. Acta Mater 2003;51:767–80. https://doi.org/10.1016/S1359-6454(02)00468-8.
[84] Kingstedt OT, Eftink B, Lambros J, Robertson IM. Quasi-static and dynamic compressive deformation of a bulk nanolayered Ag–Cu eutectic alloy: Macroscopic response and dominant deformation mechanisms. Mater Sci Eng, A 2014;595:54–63. https://doi.org/10.1016/j.msea.2013.11.061.
[85] Misják F, Barna PB, Tóth AL, Ujvári T, Bertóti I, Radnóczi G. Structure and mechanical properties of Cu–Ag nanocomposite films. Thin Solid Films 2008;516:3931–4. https://doi.org/10.1016/j.tsf.2007.07.202.
[86] Park EM, Song GA, Lee JK, Lee MH, Lee HS, Park JY, et al. Effect of solubility on strengthening of Ag–Cu ultrafine eutectic composites. J Alloy Compd 2011;509:9015–8. https://doi.org/10.1016/j.jallcom.2011.06.021.
[87] Gorsse S, Ouvrard B, Gouné M, Poulon-Quintin A. Microstructural design of new high conductivity – high strength Cu-based alloy. J Alloy Compd 2015;633:42–7. https://doi.org/10.1016/j.jallcom.2015.01.234.
[88] Senturk BS, Liu Y, Mantese JV, Alpay SP, Aindow M. Effects of microstructure on native oxide scale development and electrical characteristics of eutectic Cu–Cu6La alloys. Acta Mater 2012;60:851–9. https://doi.org/10.1016/j.actamat.2011.11.013.
[89] Perry AJ, Nicoll AR, Phillips K, Sahm PR. The copper-boron eutectic-unidirectionally solidified. J Mater Sci 1973;8:1340–8. https://doi.org/10.1007/BF00549350.
[90] Zhai W, Geng DL, Wang WL, Wei B. A calorimetric study of thermodynamic properties for binary Cu–Ge alloys. J Alloy Compd 2012;535:70–7. https://doi.org/10.1016/j.jallcom.2012.04.091.
[91] Gao H, Wang J, Shu D, Sun B. Microstructure and strength of Cu–Fe–Ag in situ composites. Mater Sci Eng, A 2007;452–453:367–73. https://doi.org/10.1016/j.msea.2006.10.111.
[92] Lebreton V, Pachoutinski D, Bienvenu Y. An investigation of microstructure and mechanical properties in Cu–Ti–Sn alloys rich in copper. Mater Sci Eng, A 2009;508:83–92. https://doi.org/10.1016/j.msea.2009.01.050.
[93] Perry AJ, Nicoll AR. Properties of alloys on the tie-line between the copper-CuZrGe pseudo-binary eutectic and the copper-Cu5Zr eutectic. J Mater Sci 1973;8:883–92. https://doi.org/10.1007/BF00553740.
[94] ASM Handbook Volume 2: Properties and Selection: Nonferrous Alloys and Special-Purpose Materials - ASM International; 1990. https://www.asminternational.org/materials-resources/results/-/journal_content/56/10192/06182G/PUBLICATION (accessed August 17, 2020).
[95] Zhang L-C. High performance ultrafine-grained Ti-Fe-based alloys with multiple length-scale phases. Adv Mater Res 2012;1(13–29). https://doi.org/10.12989/AMR.2012.1.1.013.
[96] Louzguine-Luzgin DV. High-strength Ti-based alloys containing Fe as one of the main alloying elements. Mater Trans 2018;59:1537–44. https://doi.org/10.2320/matertrans.M2018114.
[97] Zhang LC, Das J, Lu HB, Duhamel C, Calin M, Eckert J. High strength Ti–Fe–Sn ultrafine composites with large plasticity. Scr Mater 2007;57:101–4. https://doi.org/10.1016/j.scriptamat.2007.03.031.
[98] Louzguine-Luzgin DV, Louzguina-Luzgina LV, Kato H, Inoue A. Investigation of Ti–Fe–Co bulk alloys with high strength and enhanced ductility. Acta Mater 2005;53:2009–17. https://doi.org/10.1016/j.actamat.2005.01.012.
[99] Park JM, Han JH, Kim KB, Mattern N, Eckert J, Kim D-H. Favorable microstructural modulation and enhancement of mechanical properties of Ti–Fe–Nb ultrafine composites. Philos Mag Lett 2009;89:623–32. https://doi.org/10.1080/09500830903236020.
[100] Kim WJ, Kelton KF. Icosahedral and related phase formation in rapidly quenched Ti-Zr-Fe alloys. Philos Mag A 1995;72:1397–408. https://doi.org/10.1080/01418619508236263.
[101] Misra DK, Sohn SW, Gabrisch H, Kim WT, Kim DH. High strength Ti–Fe–(In, Nb) composites with improved plasticity. Intermetallics 2010;18:342–7. https://doi.org/10.1016/j.intermet.2009.08.005.
[102] Misra DK, Sohn SW, Kim WT, Kim DH. High strength hypereutectic Ti–Fe–Ga composites with improved plasticity. Intermetallics 2010;18:254–8. https://doi.org/10.1016/j.intermet.2009.07.022.
[103] Das J, Kim KB, Baier F, Löser W, Gebert A, Eckert J. Bulk ultra-fine eutectic structure in Ti–Fe–base alloys. J Alloy Compd 2007;434–435:28–31. https://doi.org/10.1016/j.jallcom.2006.08.163.
[104] Das J, Kim KB, Baier F, Löser W, Eckert J. High-strength Ti-base ultrafine eutectic with enhanced ductility. Appl Phys Lett 2005;87:161907. https://doi.org/10.1063/1.2105998.
[105] Han JH, Kim KB, Yi S, Park JM, Sohn SW, Kim TE, et al. Formation of a bimodal eutectic structure in Ti–Fe–Sn alloys with enhanced plasticity. Appl Phys Lett 2008;93:141901. https://doi.org/10.1063/1.2990662.
[106] Das J, Eckert J, Theissmann R. Structural short-range order of the β-Ti phase in bulk Ti–Fe–(Sn) nanoeutectic composites. Appl Phys Lett 2006;89:261917. https://doi.org/10.1063/1.2424274.
[107] Sueptitz R, Das J, Baunack S, Gebert A, Schultz L, Eckert J. Corrosion and pitting behaviour of ultrafine eutectic Ti–Fe–Sn alloys. J Alloy Compd 2010;503:19–24. https://doi.org/10.1016/j.jallcom.2010.05.052.
[108] Van Steenberge N, Das J, Concustell A, Sort J, Suriñach S, Eckert J, et al. Influence of annealing on the microstructure and hardness of Ti67.79Fe28.36Sn3.85 nanocomposite rods. Scr Mater 2006;55:1087–90. https://doi.org/10.1016/j.scriptamat.2006.08.036.
[109] Eckert J, Das J, Xu W, Theissmann R. Nanoscale mechanism and intrinsic structure related deformation of Ti-alloys. Mater Sci Eng, A 2008;493:71–8. https://doi.org/10.1016/j.msea.2007.08.094.
[110] Han JH, Kim KB, Yi S, Park JM, Kim DH, Pauly S, et al. Influence of a bimodal eutectic structure on the plasticity of a (Ti70.5Fe29.5)91Sn9 ultrafine composite. Appl Phys Lett 2008;93:201906. https://doi.org/10.1063/1.3029745.
[111] Samal S, Mondal B, Biswas K, Govind. Electron microscopic study on the suction cast in situ Ti-Fe-Sn ultrafine composites. Metall Mat Trans A 2013;44:427–39. https://doi.org/10.1007/s11661-012-1404-1.
[112] Mondal B, Samal S, Biswas K, Govind. Development of ultrafine Ti-Fe-Snin-situcomposite with enhanced plasticity. In: IOP Conf Ser: Mater Sci Eng 2012; 27:012025. 10.1088/1757-899X/27/1/012025.
[113] Louzguine-Luzgin DV, Louzguina-Luzgina LV, Inoue A. Deformation behavior of high strength metastable hypereutectic Ti–Fe–Co alloys. Intermetallics 2007;15:181–6. https://doi.org/10.1016/j.intermet.2006.05.006.
[114] Louzguine-Luzgin DV, Louzguina-Luzgina LV, Polkin VI, Inoue A. Deformation-induced transformations in Ti60Fe20Co20 alloy. Scr Mater 2007;57:445–8. https://doi.org/10.1016/j.scriptamat.2007.04.021.
[115] Louzguine DV, Kato H, Inoue A. High-strength hypereutectic Ti–Fe–Co bulk alloy with good ductility. Philos Mag Lett 2004;84:359–64. https://doi.org/10.1080/09500830410001728336.
[116] Louzguina-Luzgina LV, Louzguine-Luzgin DV, Inoue A. Influences of additional alloying elements (V, Ni, Cu, Sn, B) on structure and mechanical properties of high-strength hypereutectic Ti–Fe–Co bulk alloys. Intermetallics 2006;14:255–9. https://doi.org/10.1016/j.intermet.2005.06.002.

[117] Samal S, Agarwal S, Gautam P, Biswas K. Microstructural evolution in Novel Suction cast multicomponent Ti-Fe-Co alloys. Metall Mat Trans A 2015;46:851–68. https://doi.org/10.1007/s11661-014-2675-5.

[118] Samal S, Agarwal S, Biswas K. Phase evolution and mechanical properties of suction cast Ti–Fe–Co ternary alloys. Trans Indian Inst Met 2018;71:201–7. https://doi.org/10.1007/s12666-017-1174-y.

[119] Okulov IV, Bönisch M, Volegov AS, Shahabi HS, Wendrock H, Gemming T, et al. Micro-to-nano-scale deformation mechanism of a Ti-based dendritic-ultrafine eutectic alloy exhibiting large tensile ductility. Mater Sci Eng, A 2017;682:673–8. https://doi.org/10.1016/j.msea.2016.11.082.

[120] Rabadia CD, Liu YJ, Chen LY, Jawed SF, Wang LQ, Sun H, et al. Deformation and strength characteristics of Laves phases in titanium alloys. Mater Des 2019;179:107891. https://doi.org/10.1016/j.matdes.2019.107891.

[121] Liying H, Cunshan W, Jianbing Q. Microstructure and properties of Ti-Fe-Zr-Y alloys prepared by laser rapid prototyping. J Alloy Compd 2017;700:159–68. https://doi.org/10.1016/j.jallcom.2017.01.040.

[122] Han L, Wang C, Li Z. Mechanical, forming and biological properties of Ti-Fe-Zr-Y alloys prepared by 3D printing. J Mater Sci Technol 2019;35:1323–33. https://doi.org/10.1016/j.jmst.2019.01.003.

[123] Ge H, Song Q, Hu W, Zhang B, Jia Y, Liu Y, et al. Microstructures and mechanical properties of as-cast TiCuFeC alloys for biomedical applications. J Alloy Compd 2018;750:96–101. https://doi.org/10.1016/j.jallcom.2018.03.361.

[124] Sengupta B, Shekhar S, Kulkarni KN. A novel ultra-high strength and low-cost as-cast titanium alloy. Mater Sci Eng, A 2017;696:478–81. https://doi.org/10.1016/j.msea.2017.04.106.

[125] Kang LM, Yang C, Zhao YJ, Li XX, Qu SG, Zhang WW, et al. Bimodal eutectic titanium alloys: Microstructure evolution, mechanical behavior and strengthening mechanism. Mater Sci Eng, A 2017;700:10–8. https://doi.org/10.1016/j.msea.2017.05.102.

[126] Kang LM, Yang C, Wang F, Li XX, Zhu DZ, Zhang WW, et al. Designing ultrafine lamellar eutectic structure in bimodal titanium alloys by semi-solid sintering. J Alloy Compd 2017;702:51–9. https://doi.org/10.1016/j.jallcom.2017.01.257.

[127] Yang C, Kang LM, Li XX, Zhang WW, Zhang DT, Fu ZQ, et al. Bimodal titanium alloys with ultrafine lamellar eutectic structure fabricated by semi-solid sintering. Acta Mater 2017;132:491–502. https://doi.org/10.1016/j.actamat.2017.04.062.

[128] Nagarajan R, Aoki K, Chattopadhyay K. Microstructural development in rapidly solidified Ti-Ni alloys. Mater Sci Eng, A 1994;179–180:198–204. https://doi.org/10.1016/0921-5093(94)90193-7.

[129] Dong D, Zhu D, Zheng H, Wang G, Xu H, Lin F, et al. Brazing TiC/Ti matrix composite using Ti Ni eutectic braze alloy. Vacuum 2018;156:411–8. https://doi.org/10.1016/j.vacuum.2018.08.012.

[130] Piao M, Miyazaki S, Otsuka K, Nishida N. Effects of Nb Addition on the Microstructure of Ti–Ni Alloys. Mater Trans, JIM 1992;33:337–45. https://doi.org/10.2320/matertrans1989.33.337.

[131] Louzguine DV, Kato H, Inoue A. High strength and ductile bulk Ti–Ni–Cu–Nb alloy with submicron-size structure units obtained by arc-melting. J Alloy Compd 2004;375:171–4. https://doi.org/10.1016/j.jallcom.2003.11.134.

[132] Lu B-C, Wang Y-L, Xu J. Revisiting the glass-forming ability of Ti–Ni–Si ternary alloys. J Alloy Compd 2009;475:157–64. https://doi.org/10.1016/j.jallcom.2008.07.055.

[133] Lu B, Li Y, Xu J. Optimal glass-forming composition and its correlation with eutectic reaction in the Ti–Ni–Al ternary system. J Alloy Compd 2009;467:261–7. https://doi.org/10.1016/j.jallcom.2007.12.050.

[134] Barabash OM, Milman YuV, Miracle DV, Karpets MV, Korzhova NP, Legkaya TN, et al. Formation of periodic microstructures involving the L12 phase in eutectic Al–Ti–Cr alloys. Intermetallics 2003;11:953–62. https://doi.org/10.1016/S0966-9795(03)00122-5.

[135] Chen H, Weitzer F, Krendelsberger N, Du Y, Schuster JC. Reaction scheme and liquidus surface of the ternary system aluminum-chromium-titanium. Metall and Mat Trans A 2009;40:2980–6. https://doi.org/10.1007/s11661-009-0014-z.

[136] Rios O, Cupid DM, Seifert HJ, Ebrahimi F. Characterization of the invariant reaction involving the L, η, γ and σ phases in the Ti–Al–Nb system. Acta Mater 2009;57:6243–50. https://doi.org/10.1016/j.actamat.2009.08.051.

[137] Wang Q, Ding H, Zhang H, Liu S, Chen R, Guo J, et al. Growth rates dependence of macro/microstructures and mechanical properties of Ti-47Al-2Nb-2Cr-0.2Er alloy directionally solidified by cold crucible. Mater Des 2017;125:146–57. https://doi.org/10.1016/j.matdes.2017.04.013.

[138] Borisov DB, Artyukh LV, Bondar AA, Martsenyuk PS, Samelyuk AV, Tsiganenko NI, et al. Titanium-boride eutectic materials. Structure of the Ti-Nb-B alloys and phase equilibria. Powder Metall Met Ceram 2007;46:58–71. https://doi.org/10.1007/s11106-007-0011-y.

[139] Borisov DB, Artyukh LV, Bondar AA, Martsenyuk PS, Samelyuk AV, Tsiganenko NI, et al. Titanium-boride eutectic materials: Structure of titanium-rich Ti-Ge-B alloys and phase equilibria at crystallization temperatures. Powder Metall Met Ceram 2007;46:153–62. https://doi.org/10.1007/s11106-007-0025-5.

[140] Ramos ECT, Silva G, Ramos AS, Nunes CA, Baptista CARP. Microstructure and oxidation behavior of Ti–Si–B alloys. Mater Sci Eng, A 2003;363:297–306. https://doi.org/10.1016/S0921-5093(03)00650-6.

[141] Firstov SO, Horna ID, Horpenko KO, Beha MD, Koval' OYu, Kotko AV. Structure and physicomechanical properties of eutectic Ti-Si-X alloys. Mater Sci 2008;44: 342–351. 10.1007/s11003-008-9089-8.

[142] Tiwary CS, Paliwal M, Kashyap S, Pandey P, Sarkar S, Kundu I, et al. Microstructures and mechanical properties of ternary Ti–Si–Sn alloys. Mater Sci Eng, A 2019. https://doi.org/10.1016/j.msea.2019.138472. 138472.

[143] Zhang T, Yang X, Miao K, Li D, Chen S, Cui X, et al. Microstructure evolution and brazing mechanism of Ti5Si3/Ti3Al composite and Ni-based superalloy joints using Ti-Zr-Cu-Ni filler alloy. Mater Sci Eng, A 2018;713:28–34. https://doi.org/10.1016/j.msea.2017.12.049.

[144] Reed RC. The Superalloys: Fundamentals and Applications; n.d. 390.

[145] Double DD, Hellawell A. The structure of flake graphite in Ni-C eutectic alloy. Acta Metall 1969;17:1071–83. https://doi.org/10.1016/0001-6160(69)90052-2.

[146] Bingbo W, Gencang Y, Yaohe Z. High undercooling and rapid solidification of Ni-32.5% Sn eutectic alloy. Acta Metall Mater 1991;39:1249–58. https://doi.org/10.1016/0956-7151(91)90212-J.

[147] Massalski TB. Phase diagrams in materials science. MTA 1989;20:1295–323. https://doi.org/10.1007/BF02665490.

[148] Caram R, Milenkovic S. Microstructure of Ni–Ni3Si eutectic alloy produced by directional solidification. J Cryst Growth 1999;198–199:844–9. https://doi.org/10.1016/S0022-0248(98)01143-9.

[149] Yao WJ, Han XJ, Wei B. Microstructural evolution during containerless rapid solidification of Ni–Mo eutectic alloys. J Alloy Compd 2003;348:88–99. https://doi.org/10.1016/S0925-8388(02)00803-4.

[150] Dirnfeld SF, Shechtman D. Microstructure and crystallography of unidirectionally solidified Ni-W eutectic alloy. MTA 1985;16:1185–93. https://doi.org/10.1007/BF02670323.

[151] Tiwari R, Tewari SN, Asthana R, Garg A. Development of NiAl-based intermetallic alloys: effect of chromium addition. Mater Sci Eng, A 1995;192–193:356–63. https://doi.org/10.1016/0921-5093(94)03218-1.

[152] Cotton JD, Noebe RD, Kaufman MJ. The effects of chromium on NiAl intermetallic alloys: Part II. Slip systems. Intermetallics 1993;1:117–26. https://doi.org/10.1016/0966-9795(93)90029-U.

[153] Park S-J, Seo S-M, Yoo Y-S, Jeong H-W, Jang H. Statistical study of the effects of the composition on the oxidation resistance of Ni-based superalloys. J Nanomater 2015;2015:1–11. https://doi.org/10.1155/2015/929546.

[154] Johnson DR, Chen XF, Oliver BF, Noebe RD, Whittenberger JD. Processing and mechanical properties of in-situ composites from the NiAlCr and the NiAl(Cr, Mo) eutectic systems. Intermetallics 1995;3:99–113. https://doi.org/10.1016/0966-9795(95)92674-O.

[155] Walter JL, Cline HE. The effect of solidification rate on structure and high-temperature strength of the eutectic NiAl-Cr. Metall Mater Trans 1970;1:1221–9. https://doi.org/10.1007/BF02900234.

[156] Walter JL, Cline HE. Stability of the directionally solidified eutectics NiAl-Cr and NiAl-Mo. MT 1973;4:33–8. https://doi.org/10.1007/BF02649602.

[157] Sheng LY, Du BN, Lai C, Guo JT, Xi TF. Influence of Tantalum Addition on Microstructure and Mechanical Properties of the Nial-Based Eutectic Alloy. Strength Mater 2017;49:109–17. https://doi.org/10.1007/s11223-017-9848-6.

[158] Guo JT, Sheng LY, Tian YX, Zhou LZ, Ye HQ. Effect of Ho on the microstructure and compressive properties of NiAl-based eutectic alloy. Mater Lett 2008;62:3910–2. https://doi.org/10.1016/j.matlet.2008.05.038.
[159] Johnson DR, Chen XF, Oliver BF, Noebe RD, Whittenberger JD. Processing and mechanical properties of in-situ composites from the NiAI-Cr and the NiAI-(Cr, Mo) eutectic systems n.d.: 15.
[160] Inoue A, Tomioka H, Masumoto T. Microstructure and mechanical properties of rapidly quenched L12 alloys in Ni-AI-X systems. Metall Trans A n.d.:11.
[161] Nathal MV, Ebert LJ. The influence of cobalt, tantalum, and tungsten on the microstructure of single crystal nickel-base superalloys. MTA 1985;16:1849–62. https://doi.org/10.1007/BF02670372.
[162] Walston S, Cetel A, MacKay R, O'Hara K, Duhl D, Joint Dreshfield R, et al. Tenth International Symposium. TMS 2004;2004:15–24. https://doi.org/10.7449/2004/Superalloys_2004_15_24.
[163] Godecke T. Liquidus projection surface and phase equilibria with liquid of the Al-AlCo-AlNi ternary subsystem. ZEITSCHRIFT FUR Met. 1997.
[164] Grushko B, Holland-Moritz D. Decagonal quasicrystals in Al-Co, Al-Ni and in their ternary alloys. Mater Sci Eng, A 1997;226–228:999–1003. https://doi.org/10.1016/S0921-5093(96)10835-2.
[165] Liu J, Li JG. Microstructure, shape memory effect and mechanical properties of rapidly solidified Co–Ni–Al magnetic shape memory alloys. Mater Sci Eng, A 2007;454–455:423–32. https://doi.org/10.1016/j.msea.2006.11.085.
[166] Zhou Y, Nash P, Bessa SM, Ferrigatto GT, Madureira BSVP, Magalhães AS, et al. Phase Equilibria in the Al-Co-Ni Alloy System. J Phase Equilib Diffus 2017;38:630–45. https://doi.org/10.1007/s11669-017-0586-z.
[167] Kimura Y, Miura S, Suzuki T, Mishima Y. Microstructure and mechanical properties of two-phase alloys based on the B2-type intermetallic compound CoAl in the Co–Al–Ni ternary system. Mater Trans, JIM 1994;35:800–7. https://doi.org/10.2320/matertrans1989.35.800.
[168] Budberg PB. Study of alloys of the ternary system nickel-aluminum-tungsten. J Inorg Chem 1958:694–8.
[169] Milenkovic S, Schneider A, Frommeyer G. Constitutional and microstructural investigation of the pseudobinary NiAl–W system. Intermetallics 2011;19:342–9. https://doi.org/10.1016/j.intermet.2010.10.019.
[170] Gao J-J, Zhao Z-L, Wei L-F, Cui K, Liu L. Microstructure and microhardness of directionally solidified NiAl–W eutectic alloy. Rare Met 2019. https://doi.org/10.1007/s12598-019-01268-5.
[171] Milenkovic S, Coelho AA, Caram R. Directional solidification processing of eutectic alloys in the Ni–Al–V system. J Cryst Growth 2000;211:485–90. https://doi.org/10.1016/S0022-0248(99)00783-6.
[172] Misra A, Wu ZL, Kush MT, Gibala R. Microstructures and mechanical properties of directionally solidified NiAl–Mo and NiAl–Mo(Re) eutectic alloys. Mater Sci Eng, A 1997;239–240:75–87. https://doi.org/10.1016/S0921-5093(97)00563-7.
[173] Kubaschewski O. Ternary alloys, vol. 7. New York: VCH; 1993.
[174] Ferrandini P, Batista WW, Caram R. Influence of growth rate on the microstructure and mechanical behaviour of a NiAl–Mo eutectic alloy. J Alloy Compd 2004;381:91–8. https://doi.org/10.1016/j.jallcom.2004.02.052.
[175] Guo JT, Huai KW, Gao Q, Ren WL, Li GS. Effects of rare earth elements on the microstructure and mechanical properties of NiAl-based eutectic alloy. Intermetallics 2007;15:727–33. https://doi.org/10.1016/j.intermet.2006.10.020.
[176] Dirnfeld SF, Schechtman D, Mironi J. The microstructure and mechanical properties of unidirectionally solidified Ni-Sn eutectic alloy. Mater Sci Eng 1985;68:183–90. https://doi.org/10.1016/0025-5416(85)90407-0.
[177] Tang L, Zhang Z, Li S, Gong S. Mechanical behaviors of NiAl-Cr(Mo)-based near eutectic alloy with Ti, Hf, Nb and W additions. Trans Nonferrous Met Soc China 2010;20:212–6. https://doi.org/10.1016/S1003-6326(09)60123-0.
[178] Sheng LY, Guo JT, Ye HQ. Microstructure and mechanical properties of NiAl–Cr(Mo)/Nb eutectic alloy prepared by injection-casting. Mater Des 2009;30:964–9. https://doi.org/10.1016/j.matdes.2008.06.061.
[179] Sheng LY, Guo JT, Tian YX, Zhou LZ, Ye HQ. Microstructure and mechanical properties of rapidly solidified NiAl–Cr(Mo) eutectic alloy doped with trace Dy. J Alloy Compd 2009;475:730–4. https://doi.org/10.1016/j.jallcom.2008.07.109.
[180] May GJ. The influence of off-axis reinforcement on the tensile strength of an Ni-Al-Cr-C eutectic composite. J Mater Sci 1975;10:77–82. https://doi.org/10.1007/BF00541033.
[181] Chanda B, Potnis G, Jana PP, Das J. A review on nano-/ultrafine advanced eutectic alloys. J Alloy Compd 2020;827:154226. https://doi.org/10.1016/j.jallcom.2020.154226.
[182] Yang J-M, Jeng SM, Bain K, Amato RA. Microstructure and mechanical behavior of in-situ directional solidified NiAl/Cr(Mo) eutectic composite. Acta Mater 1997;45:295–308. https://doi.org/10.1016/S1359-6454(96)00124-3.
[183] Zhang J-F, Shen J, Shang Z, Wang L, Fu H. Elevated temperature tensile properties and deformation of directionally solidified NiAl–Mo in-situ composites. Mater Charact 2015;99:160–5. https://doi.org/10.1016/j.matchar.2014.11.016.
[184] West brook JH, Fleischer RL. Intermetallic compounds: principles and practice, vol. 1. John Wiley and Sons; 1995.
[185] West brook JH, Fleischer RL. Intermetallic compounds: principles and practice. vol. 2. John Wiley and Sons; 1995.
[186] Shibuya S, Kaneno Y, Yoshida M, Shishido T, Takasugi T. Mechanical properties of dual multi-phase single-crystal intermetallic alloy composed of geometrically close packed Ni3X (X: Al and V) type structures. Intermetallics 2007;15:119–27. https://doi.org/10.1016/j.intermet.2006.03.009.
[187] Shibuya S, Kaneno Y, Tsuda H, Takasugi T. Microstructural evolution of dual multi-phase intermetallic alloys composed of geometrically close packed Ni3X (X: Al and V) type structures. Intermetallics 2007;15:338–48. https://doi.org/10.1016/j.intermet.2006.08.004.
[188] Kawahara K, Kaneno Y, Kakitsuji A, Takasugi T. Microstructural factors affecting hardness property of dual two-phase intermetallic alloys based on Ni3Al–Ni3V pseudo-binary alloy system. Intermetallics 2009;17:938–44. https://doi.org/10.1016/j.intermet.2009.04.004.
[189] Wang L, Shen J, Zhang Y, Fu H. Microstructure, fracture toughness and compressive property of as-cast and directionally solidified NiAl-based eutectic composite. Mater Sci Eng, A 2016;664:188–94. https://doi.org/10.1016/j.msea.2016.04.001.
[190] Ding J, Jiang S, Li Y, Wu Y, Wu J, Peng Y, et al. Microstructure evolution behavior of Ni3Al (γ′) phase in eutectic γ-γ′ of Ni3Al-based alloy. Intermetallics 2018;98:28–33. https://doi.org/10.1016/j.intermet.2018.04.010.
[191] Lapin J. Effect of directional solidification and heat treatments on the microstructure and mechanical properties of multiphase intermetallic Zr-doped Ni–Al–Cr–Ta–Mo alloy. Intermetallics 2006;14:1417–27. https://doi.org/10.1016/j.intermet.2006.01.048.
[192] Lapin J, Mareček J. Effect of growth rate on microstructure and mechanical properties of directionally solidified multiphase intermetallic Ni–Al–Cr–Ta–Mo–Zr alloy. Intermetallics 2006;14:1339–44. https://doi.org/10.1016/j.intermet.2005.10.016.
[193] Čermák J, Rothová V. Surface barrier for hydrogen permeability in Ni3Al — influence of Cr, Fe and Zr. Intermetallics 2001;9:403–8. https://doi.org/10.1016/S0966-9795(01)00016-4.
[194] Lapin J. Embrittlement of directionally solidified Zr-doped multiphase intermetallic Ni–Al–Cr–Ta–Mo alloy after heat treatment. Scr Mater 2004;51:733–8. https://doi.org/10.1016/j.scriptamat.2004.05.051.
[195] Lee DB, Santella ML. High temperature oxidation of Ni3Al alloy containing Cr, Zr, Mo, and B. Mater Sci Eng, A 2004;374:217–23. https://doi.org/10.1016/j.msea.2004.02.012.
[196] Lee D, Santella ML, Anderson IM, Pharr GM. Thermal aging effects on the microstructure and short-term oxidation behavior of a cast Ni3Al alloy. Intermetallics 2005;13:187–96. https://doi.org/10.1016/j.intermet.2004.07.046.
[197] Gunjal VV. IISc, Bangalore, n.d.
[198] Sharma A. An evaluation of the mechanical behaviour of some new high-temmperature materials. Bangalore: IISc; 2018.
[199] Tiwary C, Kashyap S, Femi OE, Banerjee D, Chattopadhyay K. Nickel-aluminium-zirconium alloys. US9816159B2, 2017.
[200] Tiwary CS, Kashiwar A, Bhowmick S, Hari Kumar KC, Chattopadhyay K, Banerjee D. Engineering an ultrafine intermetallic eutectic ternary alloy for high strength and high temperature applications. Scr Mater 2018;157:67–71. https://doi.org/10.1016/j.scriptamat.2018.07.036.
[201] Chen Q, Huang LH, Liu HS, Zheng F, Jin ZP. Isothermal Sections of Al-Ni-Zr Ternary System at 850 and 1050 °C. J Phase Equilib Diffus 2013;34:390–402. https://doi.org/10.1007/s11669-013-0248-8.

[202] Lahiri A, Tiwary C, Chattopadhyay K, Choudhury A. Eutectic colony formation in systems with interfacial energy anisotropy: A phase field study. Comput Mater Sci 2017;130:109–20. https://doi.org/10.1016/j.commatsci.2017.01.007.
[203] Jackson MR, Bewlay BP, Rowe RG, Skelly DW, Lipsitt HA. High-temperature refractory metal-intermetallic composites. JOM 1996;48:39–44. https://doi.org/10.1007/BF03221361.
[204] Bewlay BP, Jackson MR, Subramanian PR. Processing high-temperature refractory-metal silicide in-situ composites. JOM 1999;51:32–6. https://doi.org/10.1007/s11837-999-0077-8.
[205] Tsakiropoulos P. Alloys for application at ultra-high temperatures: Nb-silicide in situ composites: Challenges, breakthroughs and opportunities. 100714 Prog Mater Sci 2020. https://doi.org/10.1016/j.pmatsci.2020.100714.
[206] Bewlay BP, Jackson MR, Subramanian PR, Zhao J-C. A review of very-high-temperature Nb-silicide-based composites. Metall Mater Trans A 2003;34:2043–52. https://doi.org/10.1007/s11661-003-0269-8.
[207] Kashyap S, Tiwary CS, Chattopadhyay K. Microstructural and mechanical behavior study of suction cast Nb–Si binary alloys. Mater Sci Eng, A 2013;583:188–98. https://doi.org/10.1016/j.msea.2013.06.045.
[208] Kashyap S, Tiwary CS, Chattopadhyay K. Effect of Gallium on microstructure and mechanical properties of Nb–Si eutectic alloy. Intermetallics 2011;19:1943–52. https://doi.org/10.1016/j.intermet.2011.05.018.
[209] Kashyap S, Tiwary CS, Chattopadhyay K. Microstructure and mechanical properties of oxidation resistant suction cast Nb–Si–Al alloy. Mater Sci Eng, A 2013;559:74–85. https://doi.org/10.1016/j.msea.2012.08.027.
[210] Tiwary CS, Kashyap S, Chattopadhyay K. Effect of Mg addition on microstructural, mechanical and environmental properties of Nb–Si eutectic composite. Mater Sci Eng, A 2013;560:200–7. https://doi.org/10.1016/j.msea.2012.09.056.
[211] Tiwary CS, Kashyap S, Chattopadhyay K. Effect of indium addition on microstructural, mechanical and oxidation properties of suction cast Nb–Si eutectic alloy. Mater Sci Technol 2013;29:702–9. https://doi.org/10.1179/1743284713Y.0000000203.
[212] Murty BS, Yeh J-W, Ranganathan S, Bhattacharjee PP. High-Entropy Alloys. Elsevier; 2019.
[213] Cantor B, Chang ITH, Knight P, Vincent AJB. Microstructural development in equiatomic multicomponent alloys. Mater Sci Eng, A 2004;375–377:213–8. https://doi.org/10.1016/j.msea.2003.10.257.
[214] Yeh J-W, Chen S-K, Lin S-J, Gan J-Y, Chin T-S, Shun T-T, et al. Nanostructured high-entropy alloys with multiple principal elements: novel alloy design concepts and outcomes. Adv Eng Mater 2004;6:299–303. https://doi.org/10.1002/adem.200300567.
[215] Ranganathan S. Alloyed pleasures: Multimetallic cocktails. Curr Sci 2003; 85: 3.
[216] Zhou YJ, Zhang Y, Wang YL, Chen GL. Solid solution alloys of AlCoCrFeNiTix with excellent room-temperature mechanical properties. Appl Phys Lett 2007;90:181904. https://doi.org/10.1063/1.2734517.
[217] Zhang Y, Zuo TT, Tang Z, Gao MC, Dahmen KA, Liaw PK, et al. Microstructures and properties of high-entropy alloys. Prog Mater Sci 2014;61:1–93. https://doi.org/10.1016/j.pmatsci.2013.10.001.
[218] Han L, Xu X, Li Z, Liu B, Liu CT, Liu Y. A novel equiaxed eutectic high-entropy alloy with excellent mechanical properties at elevated temperatures. Mater Res Lett 2020;8:373–82. https://doi.org/10.1080/21663831.2020.1772395.
[219] Miracle D, Miller J, Senkov O, Woodward C, Uchic M, Tiley J. Exploration and development of high entropy alloys for structural applications. Entropy 2014;16:494–525. https://doi.org/10.3390/e16010494.
[220] Mishra AK, Samal S, Biswas K. Solidification behaviour of Ti–Cu–Fe–Co–Ni high entropy alloys. Trans Indian Inst Met 2012;65:725–30. https://doi.org/10.1007/s12666-012-0206-x.
[221] Wani IS, Bhattacharjee T, Sheikh S, Bhattacharjee PP, Guo S, Tsuji N. Tailoring nanostructures and mechanical properties of AlCoCrFeNi2.1 eutectic high entropy alloy using thermo-mechanical processing. Mater Sci Eng, A 2016;675:99–109. https://doi.org/10.1016/j.msea.2016.08.048.
[222] Samal S, Biswas K. Novel high-strength NiCuCoTiTa alloy with plasticity. J Nanopart Res 2013;15:1783. https://doi.org/10.1007/s11051-013-1783-2.
[223] Lu Y, Jiang H, Guo S, Wang T, Cao Z, Li T. A new strategy to design eutectic high-entropy alloys using mixing enthalpy. Intermetallics 2017;91:124–8. https://doi.org/10.1016/j.intermet.2017.09.001.
[224] Jiang H, Han K, Gao X, Lu Y, Cao Z, Gao MC, et al. A new strategy to design eutectic high-entropy alloys using simple mixture method. Mater Des 2018;142:101–5. https://doi.org/10.1016/j.matdes.2018.01.025.
[225] Rahul MR, Phanikumar G. Design of a seven-component eutectic high-entropy alloy. Metall Mat Trans A 2019;50:2594–8. https://doi.org/10.1007/s11661-019-05210-3.
[226] Ding Z, He Q, Yang Y. Exploring the design of eutectic or near-eutectic multicomponent alloys: From binary to high entropy alloys. Sci China Technol Sci 2018;61:159–67. https://doi.org/10.1007/s11431-017-9051-6.
[227] Lu Y, Dong Y, Guo S, Jiang L, Kang H, Wang T, et al. A promising new class of high-temperature alloys: eutectic high-entropy alloys. Sci Rep 2014;4:6200. https://doi.org/10.1038/srep06200.
[228] He F, Wang Z, Cheng P, Wang Q, Li J, Dang Y, et al. Designing eutectic high entropy alloys of CoCrFeNiNbx. J Alloy Compd 2016;656:284–9. https://doi.org/10.1016/j.jallcom.2015.09.153.
[229] Lu Y, Dong Y, Jiang H, Wang Z, Cao Z, Guo S, et al. Promising properties and future trend of eutectic high entropy alloys. Scr Mater 2020;187:202–9. https://doi.org/10.1016/j.scriptamat.2020.06.022.
[230] Shi P, Ren W, Zheng T, Ren Z, Hou X, Peng J, et al. Enhanced strength–ductility synergy in ultrafine-grained eutectic high-entropy alloys by inheriting microstructural lamellae. Nat Commun 2019;10:489. https://doi.org/10.1038/s41467-019-08460-2.
[231] Jain R, Dewangan SK, Kumar V, Samal S. Artificial neural network approach for microhardness prediction of eight component FeCoNiCrMnVAlNb eutectic high entropy alloys. 140059 Mater Sci Eng, A 2020. https://doi.org/10.1016/j.msea.2020.140059.
[232] Wani IS, Bhattacharjee T, Sheikh S, Clark IT, Park MH, Okawa T, et al. Cold-rolling and recrystallization textures of a nano-lamellar AlCoCrFeNi2.1 eutectic high entropy alloy. Intermetallics 2017;84:42–51. https://doi.org/10.1016/j.intermet.2016.12.018.
[233] Rahul MR, Samal S, Venugopal S, Phanikumar G. Experimental and finite element simulation studies on hot deformation behaviour of AlCoCrFeNi2.1 eutectic high entropy alloy. J Alloy Compd 2018;749:1115–27. https://doi.org/10.1016/j.jallcom.2018.03.262.
[234] Samal S, Rahul MR, Kottada RS, Phanikumar G. Hot deformation behaviour and processing map of Co-Cu-Fe-Ni-Ti eutectic high entropy alloy. Mater Sci Eng, A 2016;664:227–35. https://doi.org/10.1016/j.msea.2016.04.006.
[235] Jain R, Jain A, Rahul MR, Kumar A, Dubey M, Sabat R, et al. Development of ultrahigh strength novel Fe-Co-Ni-Cr-Zr quasi-peritectic high entropy alloy by integrated approach using experiment and simulation. Materialia, Under Review 2020.